Thesis for the degree of Doctor of Philosophy

Metabolic communication between individual yeast cells

Martin Mojica Benavides

Department of Physics
University of Gothenburg

Göteborg, Sweden 2019

UNIVERSITY OF GOTHENBURG

Metabolic communication between individual yeast cells

Martin Mojica Benavides
978-91-7833-708-8 (printed)
978-91-7833-709-5 (electronic)

Department of Physics
University of Gotheburg
SE-412 96 Göteborg
Tel: +46 (0)31-7721000, Fax: +46 (0)31-7723496
http://www.physics.gu.se

Printed by BrandFactory AB
Göteborg, Sweden 2019

Metabolic communication between individual yeast cells

Martin Mojica Benavides
Department of Physics
University of Gothenburg

Abstract

With the recent progress in sensitive cell manipulation and microfabrication techniques, glycolytic oscillations in yeast have been observed at a single-cell level. It was shown that individually, oscillating cells could entrain their phases by periodic external perturbations. However, the mechanisms by which individual cells communicate to couple their glycolytic cycles within an heterogenic population remained an open question. The aims of the studies presented in this thesis focused on addressing the spatio-temporal dynamics present in the transitions from uncorrelated behaviour of individual cells, to the emergence of synchronized subpopulations and travelling waves.

In this work, it is reported the design, simulation and fabrication of microfluidic systems that allowed for the environmental control and experimental observation of glycolytic synchronization between individual yeast cells. Optical tweezers (for positioning), together with custom made microfluidic devices, were implemented to induce glycolytic oscillations in monolayered yeast cell arrangements. The developed diffusion-based chambers guaranteed the quasi-static conditions required for intercellular exchange of chemical mediators. Subsequent image and signal processing, together with graph theory, served the purpose of evaluating the degree of synchrony among individual cells and the spatio-temporal distribution of the coupling. This study shows that synchronization communities are formed depending on the exposure ratios of cyanide and glucose, and the exchanged acetaldehyde. Moreover, those communities are also defined depending on the cell location in the monolayer. The relative phase delays between the glycolytic oscillations from different communities revealed the formation of glycolytic synchronization waves, which can overcome the existing heterogeneity in the system.

The results presented in this work contribute to a further understanding on the experimental conditions required to achieve glycolytic synchronization in yeast for single-cell level studies. Furthermore, the spatio-temporal characterization of the single-cell responses during cell-cell chemical interactions, explains the formation of travelling waves as a mechanism for glycolytic synchronization. These results, and the developed methodology, can be further optimized and extrapolated to study more complicated cell systems such as the pancreatic β-cells, and the role of metabolic synchronization in the coordinated insulin secretion from the pancreas.

Keywords: Glycolytic oscillations, yeast cells, microfluidics, synchronization waves, cell-cell communication, communities, optical tweezers

This thesis is based on the work contained in the following scientific papers.

I **An optical tweezers, epi-fluorescence and microfluidic-setup for synchronization studies of glycolytic oscillations in living yeast cells**
M. Mojica-Benavides, A. A. Banaeiyan, D. D. van Niekerk, J. L. Snoep, A.-K. Gustavsson, C. B. Adiels and M. Goksör
Proceedings of SPIE, **9922**, 992218-1 - 992218-7, (2016).

II **Intercellular communication induces glycolytic synchronization waves between individually oscillating cells**
M. Mojica-Benavides, D. D. van Niekerk, M. Mijalkov, J. L. Snoep, B. Mehlig, G. Volpe, M. Goksör and C. B. Adiels
Submitted

III **Cell heterogeneity affects the formation of glycolytic synchronization waves in yeast**
M. Mojica-Benavides, D. D. van Niekerk, J. L. Snoep, B. Mehlig, C. B. Adiels and M. Goksör
Manuscript

Contents

Chapter 1

Introduction

Individual cells in nature do not live in isolation, they cooperate and coordinate to assure survival, tissue growth, or organ functionality among others [1, 2]. Their capacity to exchange information can be crucial to access nutrients, to respond to environmental changes, or to defend against viruses and disease [3, 4]. The mechanisms by which individual cells communicate can vary across species and target specific cell functions i.e. the synchronization of individual cells' energy metabolism [2, 5]. Generally, cell synchronization can occur by means of signal transduction, neural control, or the exchange of mediating molecules [6–8]. This thesis focuses on cell-cell communication and the mechanisms by which individual cells transition into a collective synchronization of their energy metabolism. Specifically, this work explores how parameters such as environmental conditions, cell-cell chemical exchange and intracellular reaction rates, influence the way individual cells adapt to each other. The universality of certain metabolic processes e.g. glycolysis, allows for biological models such as yeast to be broadly used to study and characterize specific metabolic dynamics [9]. Yeast cells are easy to handle and fast to culture, which makes them experimentally suitable before moving to more complicated cell types i.e. pancreatic β cells [10].

1.1 Glycolytic Synchronization in yeast: From a macroscopical approach, down to individual oscillating cells.

The energy metabolism in cells has as a main task to convert available nutrient sources such as glucose (GLC), into molecules i.e. adenosine triphosphate (ATP) that can provide the energy required to maintain life. The cell metabolism starts with glycolysis which takes place in the cytosol. It begins with the absorption of GLC and is followed by nine enzymatic steps. Each molecule of GLC containing six carbon atoms, breaks down into two pyruvate (PYR) molecules with three carbon atoms each. Through this pathway, the net produced energy can be quantified in terms of two available ATPs. Additionally, glycolysis produces two molecules of reduced nicotinamide adenine dinucleotide (NADH), an intermediate metabolite that serves as an electron carrier for posterior metabolic stages [2, 11]. NADH is of special interest in the scope of this work due to the fact that it is

autofluorescent and serves as a marker to track the glycolytic cycle [12, 13]. If oxygen is available, glycolysis is then followed by an oxidation process where two PYR molecules are transported to the mitochondria in the form of acetyl-coenzyme A (CoA). During this step, two new NADH molecules are created. Once the acetyl CoA reaches inside the mitochondria, the citric acid cycle or Krebs cycle starts and two new ATPs and 6 NADHs are produced per loop. The NADH produced here is consumed by the process known as the electron transport chain [14, 15]. This process can be understood as an electron valve that is able to produce two to three ATPs per NADH molecule, reaching a total of approximately 20 ATPs out of a single molecule of GLC. Alternatively, under anaerobic conditions, eukaryotic cells like yeast can force PYR into a fermentation process. Here, a final molecule of ethanol (ETHO) is produced via acetaldehyde (ACA), an intermediate metabolite that uses two available molecules of NADH and produce two new NAD+s. This NAD+ isrequired upstream the metabolic chain, which results in a feedback regulation of glycolysis [16–18].

It has been shown that when yeast cells are exposed to a mitochondrial respiration inhibitor such as cyanide (CN^-), the cellular metabolism is limited exclusively to the cytosolic activity and glycolysis becomes the dominant mechanism to produce ATP [19, 20]. During the 1950s and 1960s, periodic fluctuations in the NADH concentration were observed when exposing intact yeast cell cultures to a solution of GLC+CN^- [13, 21–24]. These phenomenon received the name of glycolytic oscillations and was reported as a synchronized response in large cell cultures. Subsequent studies showed glycolytic oscillations in cell-free extracts, where the periodicity was determined exclusively by the chemical reaction rates [25–28]. The observed divergence of the time scales present in cells-free extracts in comparison with the cell population measurements, suggested an influence of internal biological clocks on the overall spectral parameters [16]. It was until the last decade that glycolytic oscillations were studied in single cells i.e. yeast cells [29, 30]. The possibility to study glycolytic oscillations in reduced cell densities, allowed for the discrete observation rather than the average responses present in stirred population samples. Newer methods for sample preparation such as low density cell sediments [31] and alginate encapsulation [32], permitted the acquisition of metabolic signals from individual cells under static environmental conditions. By having reduced populations of yeast cells, it was possible to characterize the degree of synchrony as a function of the cell density. With the parallel advances in microfabrication techniques, microfluidic devices brought the possibility of having sensitive and dynamical control on the environmental conditions surrounding isolated yeast cells [30]. Thus, it was possible to perform perturbation studies to link external entrainment with the intracellular metabolic network. By periodically alternating flows with different concentrations of CN^- or ACA, an array of isolated yeast cells incoherently oscillating could be externally entrained [33, 34]. Synchronization studies in both, population and single-cell level have confirmed the roll of ACA as a mediator between yeast cells [35, 9]. ACA has a relatively fast diffusion through the cell membrane in comparison to the glycolytic period. In consequence, the intercellular concentrations of ACA can carry spectral information between the individual oscillating cells [30]. Moreover, cell-cell feedback system that involves the intracellular phase regulating process was revealed experimentally and numerically. Figure 1.1 shows an schematic of the principal glycolytic steps affected by incoming external ACA perturbations in a single yeast cell, where the enzyme phosphofructokinase (PFK) can be considered as the phase regulator during each

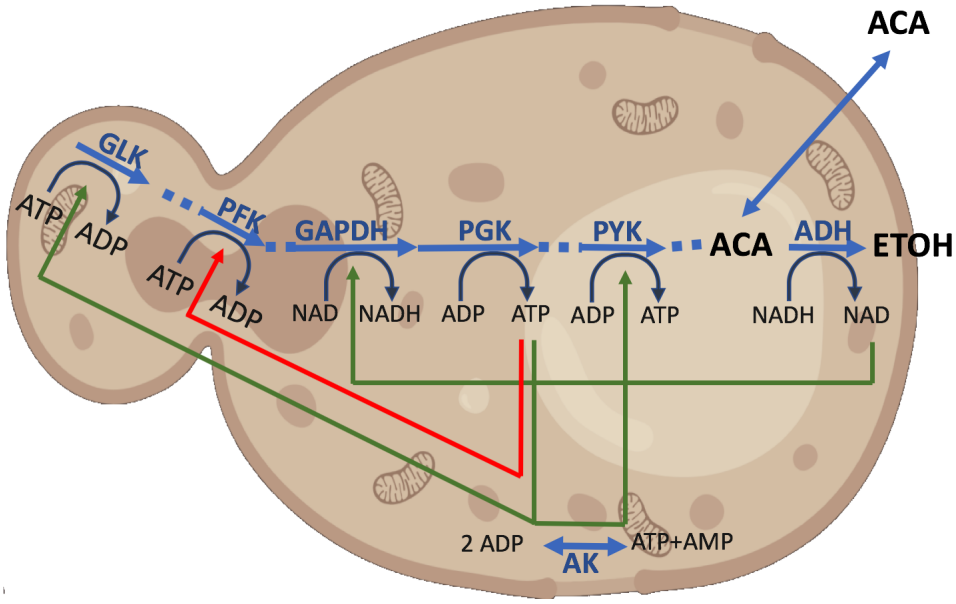

Figure 1.1: Summarized schematic of the role of external ACA as a phase-shift agent during the glycolytic cycle. The fast and easy transport of ACA through the cell membrane allows the acceleration of the alcohol dehydrogenase reaction (ADH), causing a fast consumption NADH and production of NAD. This stimulates the D-glyceraldehyde 3-phosphate dehydrogenase reaction (GAPDH) and in consequence, the subsequent phosphoglycerate kinase reaction (PGK). Therefore, the ATP concentration increases rapidly and is available for the production of ADP via adenylate kinase (AK). This results in a later ATP production through the pyruvate kinase reaction (PYK). The produced ATP can be directly consumed via the glucokinase (GLK) reaction and the phosphofructokinase (PFK) reaction. This last one (marked in red) happens significantly faster as reported in [36], making PFK the responsible enzyme for the phase shift due to exchanged ACA.

cycle [36]. Here, response curves have shown how intercellular ACA oscillations can result into a phase adaptation depending on where in the glycolytic cycle the cells are.

Up to present there is strong evidence from population and single-cell studies that ACA mediates the glycolytic synchronization. However, there is still a knowledge gap between the results obtained by single-cell analysis and the population domain. Moreover, how incoherent oscillating cells transition due to cell-cell interactions into a synchronized state, remained as an open question. Chapter 2 discusses the limitations of previous studies and motivates the experimental approach presented in this thesis.

1.2 Glycolytic synchronization waves

From cell-free extracts and population studies, it was also suggested that cell-cell communication between oscillating yeast cells can generate a spatio-temporal organization of the glycolytic oscillations [37–39]. Experimental evidence showed that under a constant supply of glucose, sustained macroscopic NADH fluorescence patterns could arise across large

cell cultures. These reports hypothesized the existence of a significantly strong coupling between the individual cells, and the observation of wavelengths around 10 cm indicated that large cell subpopulations were in the same metabolic state. However, the molecular mechanism behind these synchronization waves was not yet understood. Yeast cell-free extracts studies reported the formation of radially travelling glycolytic waves when introducing a local chemical perturbation. With the injection of fructose 2,6 bisphosphate as the main activator of PFK, it was possible to identify a spatial regulation of the glycolytic oscillations [38]. Similarly, traveling glycolytic synchronization waves were reported across cell populations immobilized in gels, with the local addition of different intermediate metabolites [40]. Nonetheless, ACA is the mediator agent for glycolysis between intact cells, and the collective regulation of PFK due to ACA signals between cells remained yet unexplained. More recent studies during the last decade, both theoretical and experimental, have aimed to characterize and model glycolytic synchronization waves in reduced yeast cells populations. The preparation of yeast cell layers in a so-called open spatial reactor [41], permitted the observation of lateral responses when exposed to sustained injections of GLC. These studies reported the influence on the wave propagation velocity not only by the intracellular parameters but by the intercellular media. In consequence, there must be a determinant coupling between the reaction-diffusion mechanisms in the environmental conditions, and the intracellular pathway that determines the spectral parameters in the propagating waves. Numerical simulations based on core models of glycolysis have characterized the responses of cell-layers in combination with external substrate gradients such as the diffusion and later absorption of GLC [42]. These simulations results concluded that the cellular periodicity is strongly influenced by the location of the specific cell within the layer. Moreover, the amplitude of the glycolytic synchronization wave not necessarily follows the decrease of the extracellular GLC but is strongly affected by the intercellular coupling. However, both the experimental and the numerical approaches to date, lack the required resolution to characterize glycolytic synchronization waves at single-cell level. The influence of cell heterogeneity and geometrical constrains, on the mechanisms behind the spatio-temporal evolution remains unanswered. Moreover, numerical simulations require a more detailed approach that allows for the connection of each individual cell's kinetic glycolytic model, with the reaction-diffusion dynamics present in the extracellular media.

On the experimental side, the work behind this thesis focuses on overcoming the limitations to sense individual cell responses during a collective behavior. For this purpose, this new approach builds on the previous study that implemented microfluidics and optical manipulation to observe single-cell glycolytic oscillations. New diffusion-based microfluidic chambers were designed, simulated and fabricated to assure the required quasi-static conditions that guarantee the cell-cell exchange of ACA while having a constant supply of GLC. Chapters 3 explains the methodology to obtain such environmental control and cell arrangement, and Chapter 4 elaborates on the experimental protocols followed to induce and measure glycolytic synchronization from single-cell signals.

The numerical simulations are presented in this work to obtain a comparative analysis between the measured cell-cell dynamics, and the collective responses using a kinetic model for oscillating single yeast cells [18]. The simulations consider the geometrical constrictions of the microfluidic chamber to calculate the concentration gradients of the extracellular media. Thus, the chemical reaction-diffusion processes present in both, the external GLC+

CN^- supply and secreted metabolites i.e. ACA and ETHO, are coupled with the intracellular glycolytic reaction chain of each cell in the array. Chapter 5 shows the implemented criteria involved in these simulations to emulate the experimental scenario, together with a deeper exploration on the parameters that influence the spatio-temporal behavior of glycolytic synchronization.

The data analysis constitutes an important contribution of this work. To date, glycolytic synchronization has been evaluated in terms of the Kuramoto order parameter [43–45]. It provides a statistical comparison on the degree of synchrony among individual oscillating cells. In order to obtain a spatio-temporal description of the cell-cell communication in a monolayered cell arrangement, graph theory is implemented for the first time to characterize cell-cell glycolytic coupling. Synchronization communities can be identified from optimization of the modularity, a measure of how well a network can be divided in subgroups based on the interconnection strengths [46–48]. In addition, this work proposes a novel way to characterize glycolytic waves by combining graph theory with delayed cross correlations of the single-cell signals. Chapter 6 describes the way experimental and simulated data is treated to describe the spatial distribution and evolution of glycolytic synchronization across the mesoscopic cell array.

Chapter 2

Motivation and Aims

Since the first studies on glycolytic oscillations in yeast, an important motivation was driven by the possibility of understanding energy metabolism as a cell-cell communication mechanism. These studies have aimed to start with simple cell models like yeast cells to more complicated systems [49,50]. In human pancreatic islets, the pulsatile insulin secretion has been related to the degree of glycolytic synchronization between individual cells [8, 10, 51–53]. The understanding of the mechanisms involving cell-cell coupling provides a new approach to explain diseases such as type II diabetes, where abnormal insulin secretion suggests a lack of synchrony between metabolic states in β cells. Population studies have shown that cell populations oscillate in phase [7], but single-cell studies have demonstrated that isolated cells can also show individual glycolytic oscillations [29, 33]. Moreover, it has been observed that dense cell layers can display spatio-temporal patterns of metabolite concentrations in the process of synchronization [39, 41]. The current available advances in single-cell studies with sensitive cell handling techniques such as microfluidics and optical manipulation [9, 30], opened the possibility to track individual cell responses to environmental perturbations. With the possibility to externally entrain individual oscillating cells, new questions arose which are addressed in this thesis:

- *Is it possible to induce and observe glycolytic synchronization at an intermediate domain between population and single-cell scales?*

  This aim focuses on the experimental conditions required to sense cell-cell synchronization in a mesoscopic array of cells. The previous microfluidic approach implemented for single-cell oscillations relies on a flow-based manipulation of the environmental conditions. Thus, the secretions from the isolated cells are washed away and it is not possible to induce cell-cell communication. This thesis work focuses on the design of a microfluidic platform that fulfill three main objectives: 1) Obtain a monolayer arrangement of the yeast cells. The idea of having 2D configuration limits the cell-cell interactions only to lateral coupling in a single plane. This provide a cell-cell observation in comparison to previous studies on macroscopic cell layers. 2) Create a geometrical constraint for the diffusion of external substrates such as GLC and CN^- , where the exposure of cells to a given concentration is linked to their location within the diffusion gradients. 3) Guarantee mechanical quasi-static conditions in order to permit the cellular exchange of mediating molecules i.e. ACA.

This aim is addressed in **Paper I** and **Paper II**.

- *How incoherent individual cells transition to a synchronized population? What are the parameters determining the emergence of synchronized subpopulations?*

  This aim focuses on studying the single-cell interactions with the media and with neighboring cells. Previous studies have shown single cell-cell synchronization as a function of cell density. However, the spatial distribution of the synchronization states has not yet been reported at this reduced scale. The influence of the external stress concentration on the spatial distribution of cell-cell synchronization is investigated in this work experimentally and with the numerical simulations. This aim is addressed in **Paper II** and **Paper III**.

- *Are glycolytic synchronization waves observable at a mesoscopic scale? How the cell heterogeneity present at single-cell level affects the robustness of phase propagation?*

  This aims focuses on the spatio-temporal characterization of glycolytic synchronization. The concentration gradient in the injected substrate suggests a relative delay in the triggering of the glycolytic oscillations. With the cell heterogeneity present in the array in terms of, age, size and enzymatic concentrations among others, whether the initial relative phase delay overcomes the initial individual phases, amplitudes and natural frequencies, constitutes the target of this part of the study. The propagation of glycolytic synchronization waves are strongly linked to the extracellular diffusion. Hence, the effect of local concentrations over the wavefront profiles is also investigated. This aim is addressed in **Paper II** and **Paper III**.

The universality of glycolysis among species constitutes a great motivation to answer these questions. The understanding of the mentioned aims can set the basis for further experiments involving relevant cell types in medicine such as the above mentioned pancreatic β-cells and cancer tumor cells.

Chapter 3

Methods

Efficient control of the environmental conditions together with sensitive cell handling is required for inducing glycolytic oscillations in both single cells and compact 2D arrangements. To achieve this, custom-made microfluidic devices were designed and fabricated. An optical trapping configuration was coupled with the microfluidic system to manipulate single cells and position them based on the surroundings and intercellular distance requirements. Images were acquired using transmission and fluorescence microscopy to detect the concentration fluctuations of NADH. This section describes the main principles and considerations behind optical and microfluidic manipulation required for cell handling during the experiments. The fabrication of microfluidic devices in **Paper I** and **Paper II** , follow a well established protocol that required posterior optimisation depending on the specific conditions. The major part of this section is extracted from the reported methods present in the previously defended licentiate thesis [54]. Additional material corresponds to new procedures implemented in the later studies.

3.1 Optical trapping for cell placement

Given the experimental conditions where individual cells are suspended in a closed microfluidic system, a contact-free manipulation tool is suitable for contactless handling of individual cells inside the device. In single-cell studies and cell-cell interaction experiments, intercellular distance constitutes a crucial parameter when controlling the required exchange of metabolites between cells. Single cells can be trapped, moved, and fixed in specific locations that correspond to required surrounding conditions. A single-trap optical tweezers consists of a laser beam focused on a sample using a high numerical aperture (NA) objective lens [55]. Due to light-matter interactions, resulting forces can trap suspended dielectric microparticles [56].

Depending on the size of the particle, the trapping forces can be described in two domains. The most generalized case is the analysis of a spherical particle. If $r \ll \lambda$, where λ is the incident wavelength and r is the particle's radius, the distinction between the components of refraction, reflection and diffraction can be neglected taking into account that the perturbation of an incident wavefront is minimal (the Rayleigh regime). In this domain, the resulting force can be divided into two components: A scattering force, which is the result of an isotropic re-emission of an incident beam, and a gradient force that

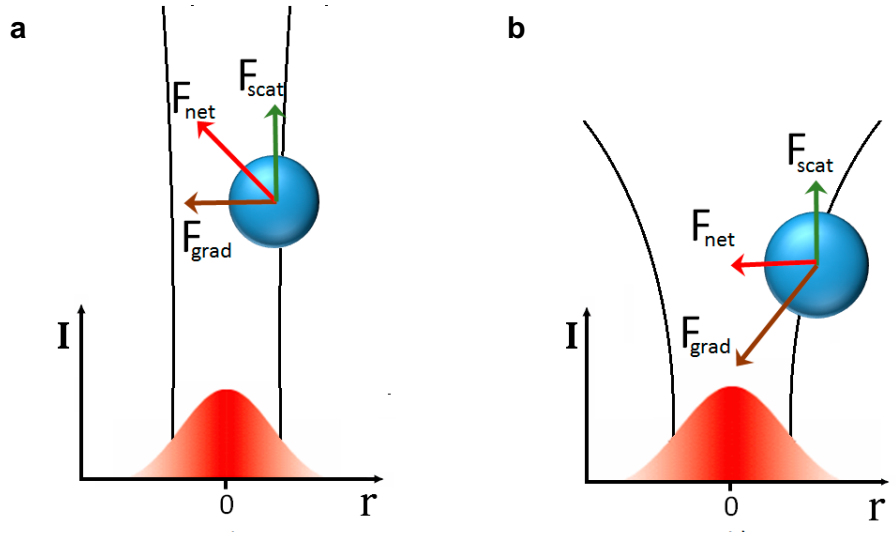

Figure 3.1: Rayleigh regime for a) slightly focused and b) tightly focused beam. In both cases the scattering and gradient force components give a resulting force. Only for b) it results into a trapping force.

considers a dielectric particle as a dipole experiencing an electromagnetic field, and which is directed towards the region of maximum intensity (see figure 3.1). For the regime where $r \gg \lambda$, ray optics approximation is suitable and the behavior of the light field obeys to the Fresnel conditions in each of the particle-surroundings interfaces [57]. These interactions result in a transmitted momentum from the photons to the particle, which is proportional to the light intensity [55,58,56]. When the rays pass through a dielectric, spherical particle with a refractive index n greater than its surrounding medium, they experience refraction and reflection. The force component for this case can be understood as the scattering force previously mentioned. The particle can also be described as a microscopic lens that

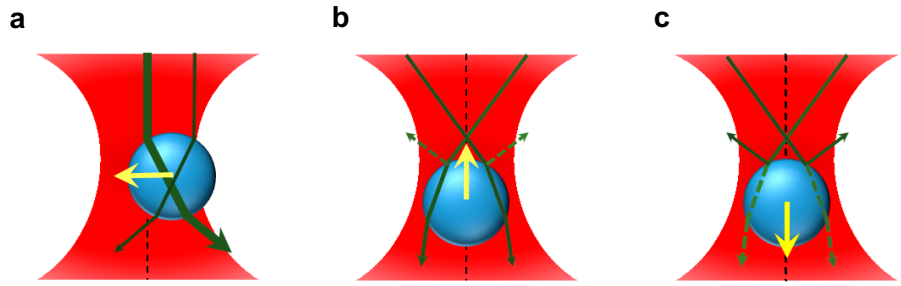

Figure 3.2: Resulting forces in the ray optics regime. a) shows the resulting force towards the region of highest intensity, b) and c) show the net forces that result into trapping.

focuses the light field. This focusing effect in addition to the momentum variation, causes the particle to move to the region of highest light intensity, analogue to the gradient force in the dipole case (see figure 3.2). If the trapped particle radius is in the order of the wavelength, a combined regime known as the Lorentz-Mie regime describes the forces involved when trapping particles of various sizes with a Gaussian beam [55, 58, 56].

Photodamage and thermal alterations need to be considered in terms of the wavelength, power, and trapping time of the designed tweezers when handling living cells. The far-infrared window has been proven to be the most suitable spectral range for optical manipulation of living samples due to the relative weak absorption by water and intracellular chromophores [59,60]. In the experiments for **Paper I**, cells were trapped for less than 5 s using a 1070 nm laser with an output power of 240 mW. These settings have been proven to maintain cell viability after a trapping time of 10 minutes [61].

3.2 Microfluidic systems

To experimentally address single-cell responses, it is crucial to have control over the environmental, chemical and mechanical activities. If each individual cell is considered as a transfer function, the provided input is considered to be the media in which it is suspended, and any changes in the environmental conditions will have an impact on the measurable feedback. The microfluidic domain offers the possibility to work with laminar flows that assure parallel velocity trajectories to the surfaces the fluid is bound with [62,63]. In contrast to the turbulent flows present in macroscopical systems where inertial forces dominate, laminar conditions permit the prediction of parabolic velocity profiles as a result of the capillary and viscous forces involved. The fluids in this work are considered as Newtonian and incompressible, hence, the density and viscosity are independent of the pressure and flow velocity respectively [64, 65]. A relation that illustrates the influence of the inertial and viscous forces on the fluid velocity, $\mathbf{u}$, for this case is the Navier-Stokes equation.

$$\rho\left(\frac{\delta \mathbf{u}}{\delta t} + \mathbf{u}\cdot\nabla\mathbf{u}\right) = -\nabla p + \eta\nabla^2\mathbf{u} + \mathbf{f} \tag{3.1}$$

where $\mathbf{f}$ stands for the body-force forces such as gravity, ρ is the fluid density, p represents the pressure and η is the dynamic viscosity. The first and second term on the right side of eq. 3.1 describe the pressure and viscous forces, respectively. The left side corresponds to the inertial components, where the first term can be neglected for the stationary case. When designing microfluidic devices, a reliable procedure to guarantee that the resulting flows fulfil laminar conditions is the calculation of the Reynolds number. It is defined as the ratio between the inertial and the viscous forces:

$$Re = \frac{\left(\rho\frac{u_0^2}{L}\right)}{\left(\eta\frac{u_0}{L^2}\right)} = \frac{\rho u_0 L}{\eta}, \tag{3.2}$$

where L corresponds to the particular length scale and u_0 is the velocity going through the device cross section. The length scale can be obtained from hydraulic diameter, D_h,

and in the case of a fully filled rectangular channel with dimensions a and b, it can be defined as

$$L = D_h = \frac{2ab}{a+b}. \tag{3.3}$$

Flows are considered to be laminar for Reynold numbers below 2300. The inertial forces above this number start to induce turbulence [66]. For the particular devices implemented in this thesis, the Reynold numbers are four orders of magnitude below this threshold, guaranteeing well defined laminar flows.

Together with the flow conditions of the liquids surrounding the cells, concentration distributions and diffusion are crucial when studying and controlling the interactions of individual cells with the media and among each other. The flux of particles, $\mathbf{J}$, from a higher to a lower concentration, c, can be estimated by the Fick's law of diffusion [67] :

$$\mathbf{J} = -D\nabla c, \tag{3.4}$$

where D is the diffusion coefficient. On the other hand, convection is the process by which particle transport is due to flow, and this flux can be expressed as $c\mathbf{u}$. In order to cover the complete mechanisms, the combination of the convective flux and the Fick's law in the continuity equation yields

$$\frac{\delta c}{\delta t} = -\nabla \cdot (-D\nabla c + c\mathbf{u}). \tag{3.5}$$

Analogously to the Reynolds number, one can determine whether the dominant particle transport mechanism is convection or diffusion by calculating the Péclet number:

$$Pe = \frac{u_0 D_h}{D}. \tag{3.6}$$

If $Pe < 1$, the particle transport rate is higher by diffusion [68]. This is the case for the devices reported in **Paper I** and **Paper II** that describe the implementation of diffusion chambers aimed to achieve quasi-static conditions.

3.3 Microfabrication of microfluidic devices

With the scaling-down of technology and the possibility of understanding the physical and biological phenomena taking place at the micron and sub-micron level, micro-fabrication techniques have become a determinant tool for scientific studies. Photolithography, in combination with soft lithography, has become a powerful technique for microfluidics development. By radiating with a plane UV light source, a light-sensitive material can be patterned using a high-resolution mask, and with additional chemical treatment, micro- and nanoscopic features can be obtained [69]. This process can be performed multiple times in order to obtain the desired number of features and layers. Polydimethylsiloxane (PDMS) is a well-known biocompatible polymer that can be molded with micron resolution, and due to its transparency, it can be used for optical imaging and manipulation [70, 71]. Figure 3.3 summarizes the procedure by which microfluidic chambers were fabricated for the studies in this work.

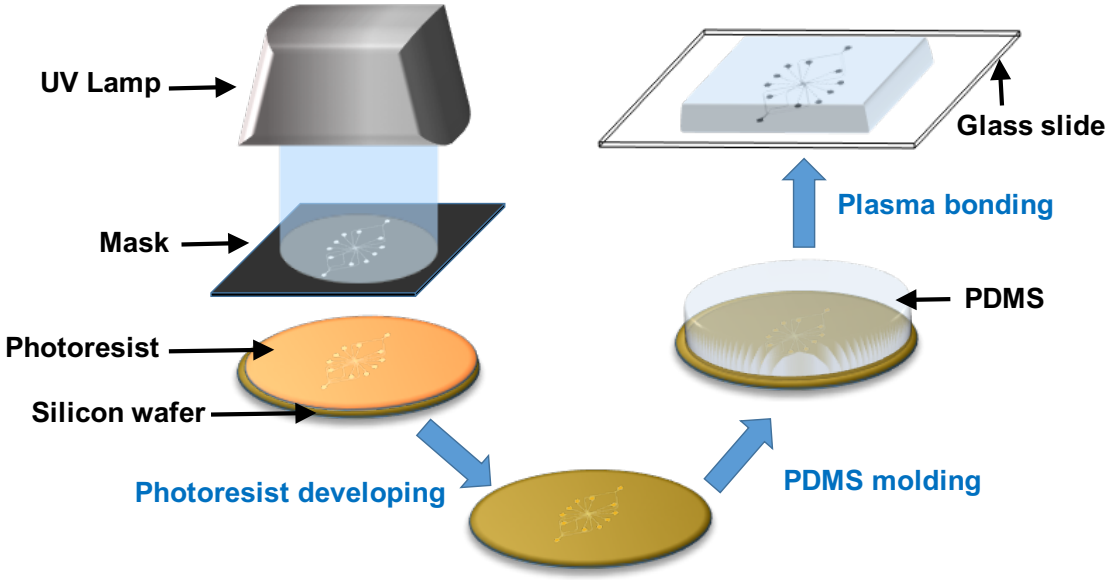

Figure 3.3: Summarized procedure for PDMS microfluidic chips. In a mask aligner, the UV lamp imprint on the photoresist the transmitted pattern from the chrome mask. After chemical development, the master is ready for PDMS molding. Finally, the obtained replica is cleaned, punched and plasma bonded to a cover glass.

Chapter 4

Experimental Procedures

4.1 Design and numerical optimization of the microfluidic chambers

The experimental procedures implemented in **Paper I** and **Paper II** required the customized design of microfluidic systems prior to fabrication. In this way, it was possible to guarantee the required sensitive handling of single cells and the precise control on the environmental conditions. The microscopic geometric features of the devices were designed using the computer-assisted drawing (CAD) software AutoCAD (Autodesk Inc., CA USA). To predict and optimize the experimental conditions such as the flow rates and diffusion of chemical species, the designs were simulated using the finite element based software COMSOL Multiphysics (COMSOL Inc., Burlington, MA, USA). Incompressible and Newtonian liquids were selected together with the "Convection-Diffusion module" to fulfill the considerations mentioned in the previous section. No-slip boundary conditions were defined for every wall limiting the system and no body forces were taken into account. The numerical interpolation was calculated using the COMSOL "Extra fine" Physics controlled mesh on the real scaled CAD designs. The boundaries corresponding to the inlets were defined with the required flow rate and the outlets' pressure was adjusted to 0 Pa. Flow velocities were calculated under stationary conditions and the results were implemented in eq. 3.5 to obtain the time-dependent concentration distributions. The transport of chemical species was tested using the diffusion of CN^- due to its higher value of the diffusion coefficient ($20.7 \text{x} 10^{-10}$ m^2/s) in comparison with GLC ($6.7 \text{x} 10^{-10}$ m^2/s).

4.1.1 Diffusion chamber for optical tweezers-assisted positioning

As a first approach to study possible intercellular interactions, a microfluidic device was designed and simulated for the experiments reported in **Paper I**. The aim was to translate the cell configuration used in previous 3-inlet microfluidic chamber experiments [9] to an environment that allows the reabsorption of secreted metabolites by neighboring cells in an array. This approach requires diffusion as the dominant mechanism for chemical transport. Thus, it is possible to replace the external perturbations achieved using

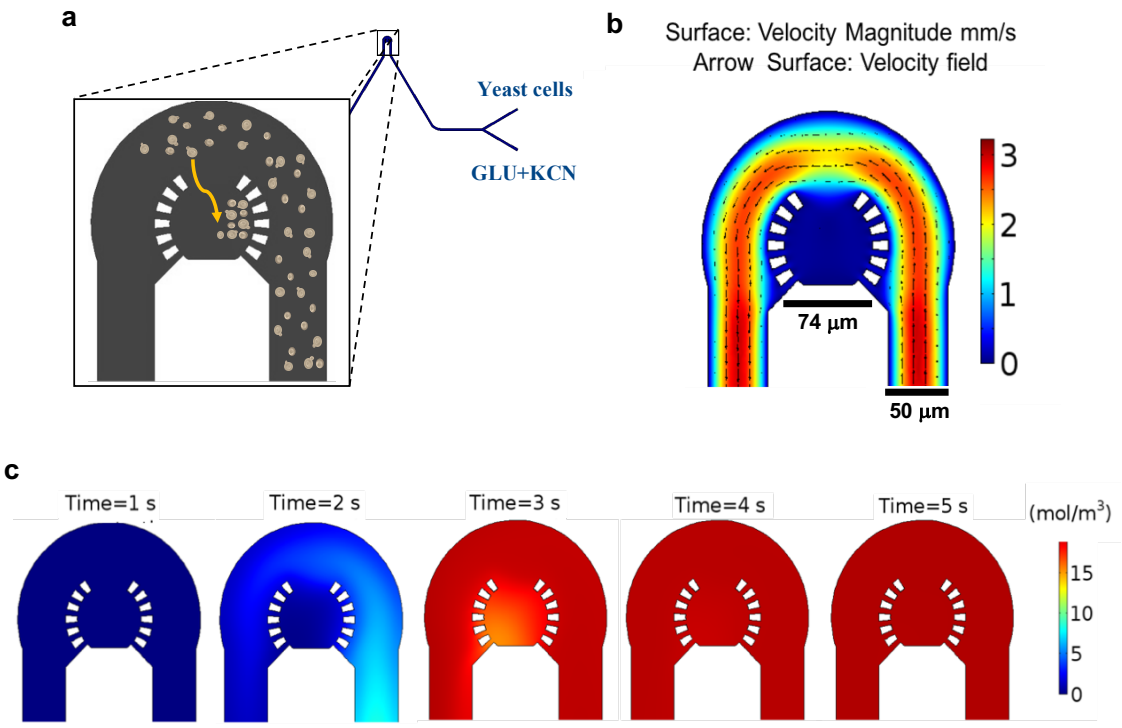

Figure 4.1: Working principle and simulations of the diffusion chamber, designed for cell positioning with optical tweezers. In a) The cells and stress solution inlets are displayed, and a zoom in the diffusion chamber shows the working principle during the cell arrangement step. Cells are optically trapped when passing the top opening in the diffusion channels, and placed in a rectangular array. The second step was simulated to evaluate the b) velocities and the c) time dependent concentration distribution during the stress injection. The velocity field showed a quasi-static behavior inside the cell chamber and the KCN concentration increased from right to left and achieved a total coverage of the injected molarity in less than 5 seconds.

the 3-inlet microfluidic chamber, with the intercellular interactions required for cell-cell synchronization. As shown in Figure 4.1a, the device has two 50 μm wide inlets for cell injection and GLC+CN^- stress solution, respectively. A 74 μm diameter circular chamber surrounded by 5 μm apertures was designed to observe cell responses when stressed by diffusion in a quasi-static environment. Analogously to the 3-inlet system, the flow-rates were adjusted for the cell arrangement and the later stress exposure. These two processes can be performed using the same channel for the two consecutive steps. First, initial input flow-rates of 50 and 0 nL/min were adjusted for the cell solution and GLC+CN^- inlets, respectively, to trap individual cells and place them inside the diffusion chamber through the top opening. Secondly, the input flows were changed to 0 and 30 nL/min for the cell solution and GLC+CN^- inlets, respectively. As previously mentioned, concentration distributions were calculated with the diffusion coefficient of CN^-.

The height of the device was fixed to 15 μm based on the required balance between

having a more compact environment to reduce the diffusing away of cells' ACA secretions, and the minimum spacing for the optical manipulation of suspended cells. The velocity field simulations showed mechanical flow around the circular chamber and quasi-static conditions in the region were the cells are arranged. The calculated time-dependent concentration distribution shows full coverage of the diffusion chamber after 5 s. Simulations were performed for 20 mM CN^- input concentration (see Figure 4.2c).

4.1.2 Diffusion chambers in the "5-in-1" device for synchronization studies

In **Paper II**, a new microfluidic chamber was designed to study glycolytic synchronization due to cell-cell communication. The device was intended to obtain a monolayer of compactly arranged cells. Therefore, it was necessary to reduce the height of the previous diffusion chamber to the average diameter of a single cell: 5 μm. With this spacing between the top and bottom surfaces of the device, optical tweezers were no longer an option for the cells' arrangement. A new inlet was added for loading the cells directly into the diffusion chamber, and the complete region was surrounded with 2 μm diffusion apertures. In contrast to the previous rectangular cell arrangements, cells should occupy the enclosed region showing radial symmetry. A cylindrical pillar was placed in the center of the circular chamber to assure good aspect ratio and have a constant height in the complete region. Therefore, this pillar helps with the homogeneous distribution of cells during the loading. Figure 4.3a shows a schematic of the working principle of the diffusion chamber.

Velocity field simulations were performed with an input flow rate of 25 nL/min. As in previous device simulations, there is a flow circulating around the cell chamber while having quasi-static conditions in the center of the device. To study the effect of the different concentration ratios between GLC and CN^- on synchronization, the device contained five different chambers for simultaneous experiments with 8, 12, 16, 20 and 24 mM input CN^- concentrations (as described in the results section in **Paper II**). The simulations for the different CN^- input molarities showed the same rates with scaled concentration values. This means that the full coverage with the input CN^- concentration was reached at the same time in all of the cases. The diffusion simulation in Figure 4.2c corresponds to the 20 mM CN^- input concentration. Compared to the simulations displayed in Figure 4.1c, diffusion through the 2 μm apertures resulted in a more homogeneous concentration distribution inside the cell region.

4.2 PDMS microfluidic chambers

The two devices implemented in the studies reported in this thesis were fabricated using the same main steps (see Figure 3.3) and equipment. However, parameters were optimized for each of the designs depending on the height of the channels and the required features resolution. The UV exposures were performed using a MA-6 mask aligner (Suss MicroTec, Germany) using an intensity of 6 mW/cm^2, with broadband emission comprising wavelengths of 365 nm (i-line), 405 nm (h-line), and 436 nm (g-line). The negative epoxy SU8

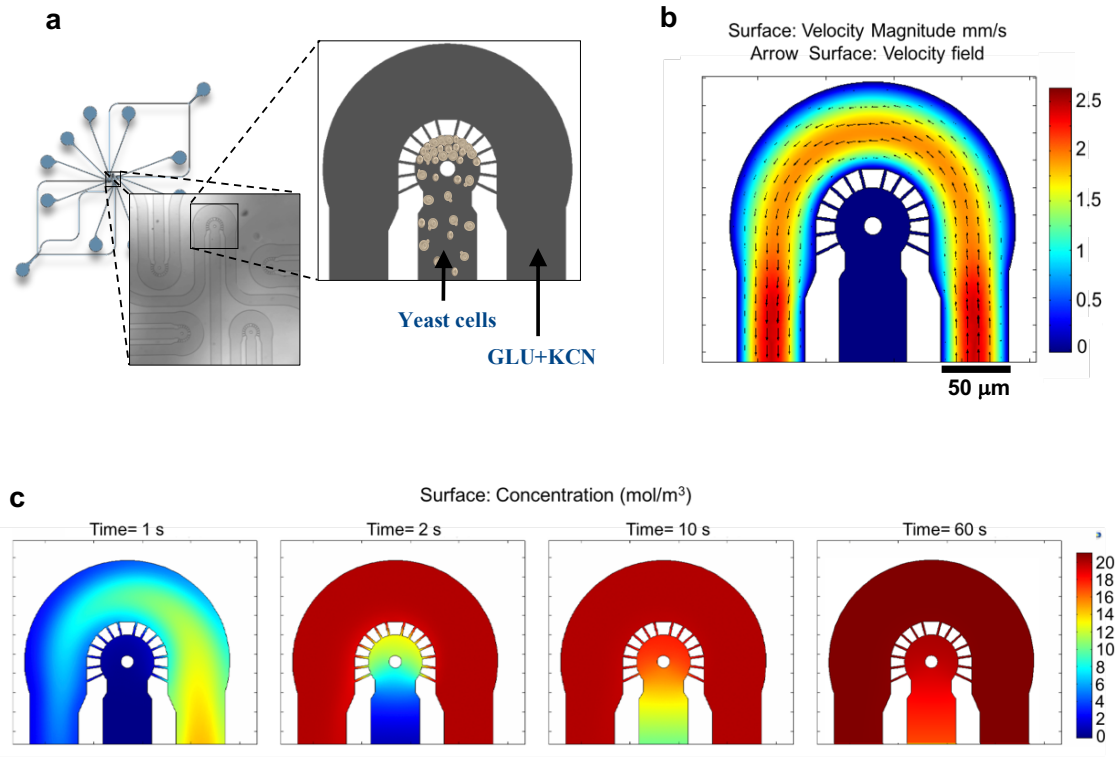

Figure 4.2: Design and microfluidic simulations for the diffusion chambers in the 5-in-1 device. In a), the configuration of the device is zoomed in to illustrate the cell loading principle and stress injection for each chamber. b) Flow velocities calculations assured the required quasi-static conditions inside the diffusion chamber and in c) time dependent concentration distributions showed the diffusion-based transport of the 20mM of KCN into the cells region. 2 μm diffusion channels induced a homogeneous and more symmetrical concentration variation in comparison with the previous design.

photoresists were implemented in the fabrication of the masters, which are photosensitive to the i-line.

Diffusion chamber for optical tweezers-assisted positioning: The channels' height was required to be 15 μm in this case. For this purpose, SU8 2015 photoresist (MicroChem Corp., Newton, MA, USA) was spin-coated at 3500 rpm on a *3-inch* silicon wafer <1,0,0>. Subsequently, the coated wafer was soft-baked at 65° C and 95° C for 2 and 3 minutes respectively. Taking into account that 5 μm is in the resolution limit of plastic masks, a chrome mask was implemented during the UV exposure step, and the mask aligner was adjusted in "Lo-vac" mode (low vacuum conditions) for 8 seconds of exposure. These parameters were optimized from the SU8 data sheets due to the sensitivity of the process. The post-exposure bake (PEB) times that showed the best performance were 3 and 6 minutes at 65° C and 95° C respectively, before the final development in mr-Dev 600 (MicroChem, Germany)..

The molding procedure was based on the procedures, as reported earlier [71, 72]. The PDMS was mixed with a crosslinker (Sylgard 184 Silicone Elastomer Kit, Dow Corning Corp. Seneffe, Belgium) in a 15:1 ratio and placed in a vacuum desiccator (Z119016, Sigma Aldrich, Germany) for approximately 30 minutes, until no bubbles that could result in obstacles in the channels could be observed. The homogenous mixture was then poured into a fixed cast surrounding the device features on the master. The system was placed in the oven at 90° C for 3 hours and then punched for posterior tubbing. After carefully cleaning the peeled PDMS solid replica with IPA and ETOH, it was plasma cleaned in a PDC-32G; 115/230V (Harrick Plasma, Ithaca, NY, USA) together with a glass cover slip for 40 s. The PDMS and the cover slip were then put together in a covalent bond due to the generated oxygen plasma. An additional baking of one hour was performed before the device was ready for experiments.
"5-in-1" device for synchronization studies: The fabrication of this system required a channel height of 5 μm. Hence, a 4-inch wafer was spin-coated with SU8 3005, which can give features of approximately 4 μm high. The photoresist was centrifuged on the wafer at 3700 rpm, followed by a soft bake of 3 and 4 minutes at 65° C and 95° C, respectively. The parameters adjusted in the mask aligner were the same as for the diffusion chamber for optical tweezers. PDMS molding was performed following the exact same procedure as for the 15 μm device.

In order to test the functioning of the fabricated microfluidic devices implemented in **Paper I** and **Paper II**, the respective chambers' diffusion was tested with uranine 10 μM. Both devices were loaded with cells as in a normal experiment. As seen in Fig. 4.3, the diffusion of the dyes takes place over different time scales due to the differences in the diffusion channels and due to the chamber in Fig. 4.3b being compactly loaded with cells.

4.3 Cell preparation and environmental control

The yeast cell strain used for the experiments was the X2180 *Saccharomyces cerevisiae*, following the procedure established earlier [73, 74]. Isolated colonies were cultured at 30° C and suspended in yeast nitrogen base (YNB) under semi-aerobic conditions. The cells were grown in a rotary incubator until the available GLC in the media was depleted. Glucose test sticks were used to periodically measure the GLC levels and observe when the solution became exhausted, meaning that the cells have achieved the diauxic shift. After the test sticks showed GLC levels under 0.1%, cells were placed back in the incubator for an additional 15 minutes in order to assure total GLC consumption. The cells were washed twice in potassium phosphate-buffered saline (PBS) and re-suspended in new PBS. The cells were starved in the rotary shaker for 3 h, washed again in PBS and stored at 4° C for 15 minutes before the experiments.

The intercellular interactions studied in **Paper I** required optical tweezers for cell positioning. This microfluidic device was pretreated with Concanavalin A (ConA), a carbohydrate-binding protein to fix the cells to the glass after placing them with the optical tweezers. This procedure was performed 30 minutes before running the experiments. The injection of the cells into the devices and the inflow control on the different stress solutions

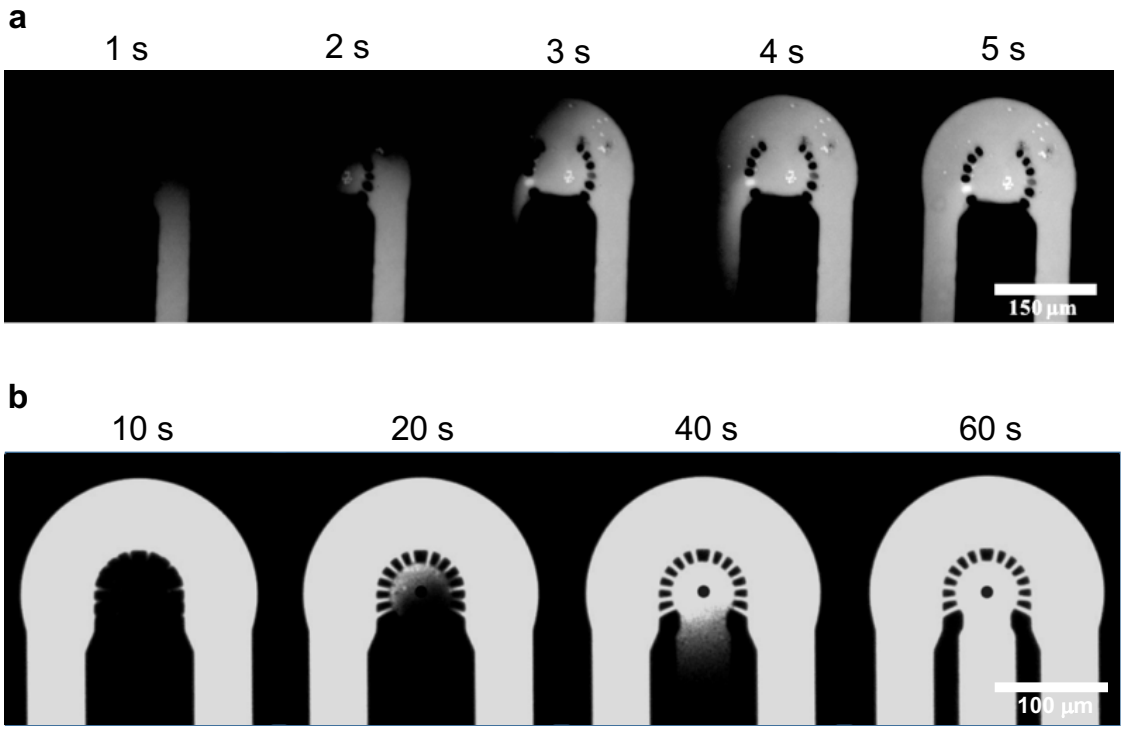

Figure 4.3: Fluoresceine testing of the diffusion chambers. The chambers implemented in a) **Paper I** and b) **Paper II** where loaded with cells as in the correspondent experiments and the diffusion was tested using the same initial conditions as in the numerical simulations. The difference in the coverage rate can be explained by the difference in the boundaries of the cell region.

in all of the experiments, was achieved with high precision multi-syringe pumps (CMA 400, CMA Microdialysis).

4.4 Optical manipulation and imaging

In order to obtain the cell arrays required for the studies performed in **Paper I**, the IR fiber laser was coupled to a 100x and 1.33 N.A. oil immersion objective mounted in an inverted microscope (DMI 6000B, Leica Microsystems). The XYZ displacement of the trap was controlled with a customized OpenLab® automation that allowed to set the trapping and positioning zones, path and number of cells in the array as well as their separation distance.

A well-known method to track glycolytic oscillations, is the acquisition of NADH autofluorescence [2]. Figure 4.4 shows the excitation and emission bands for NADH, showing a peak of excitation in the UV range. To achieve excitation and be able to detect the emitted fluorescence, a DAPI filter cube (excitation filter 350/54 nm and emission filter 415/64; 49000-ET-DAPI, Chroma) was mounted in the inverted microscope mentioned previously

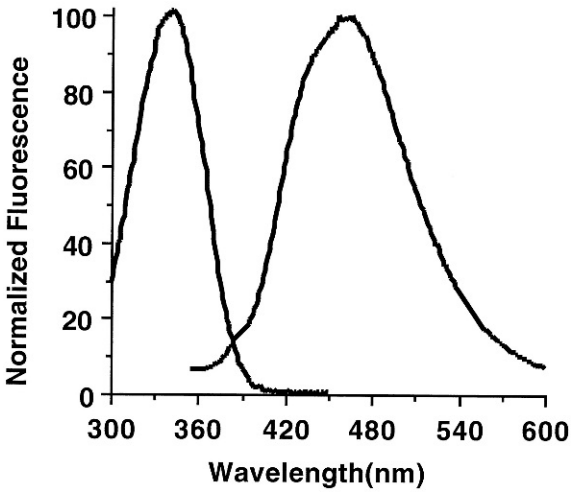

Figure 4.4: Excitation and emission spectra for NADH autofluorescence. The excitation band shows a maximum at 340 nm and the emisission at 460 nm, however, the emission when using a DAPI filter is still very weak and a high sensitive EM-CCD is required for the acquisition. Copyright (2000) National Academy of Sciences, USA.

for optical trapping. In this way, the filtered illumination of a mercury lamp (EL6000; Leica Microsystems) excited the NADH molecules in the cells and the fluorescence was confocally collected with an EM-CCD camera (C9100-12; Hamamatsu Photonics, Shizuoka, Japan). Figure 4.5 shows a schematic of the complete optical setup.

Excitation time and power are crucial parameters to take into account when dealing with biological samples. High powers or prolonged exposures can result in alterations of the fluorescent molecules known as photobleaching [75,76]. The excitation power from the lamp was adjusted to 15 W for all the experiments, and the exposure time was 400 ms.

An OpenLab routine was used for the exposure and sampling of the NADH responses. For the synchronization studies in **Paper I** and **Paper II**, simultaneous excitation and acquisition of fluorescence images were performed every 2 seconds. Taking into account that the typical frequencies in glycolytic oscillations are around 0.015 to 0.033 Hz, the sampling frequency obeys the Nyquist optimal sampling rate [77]. For the experiments with the "5-in-1" device images were acquired moving through all the chambers in the device, in a closed circular loop as part of the automation routine, guaranteed the same distance and time for all the imaging positions.

4.5 Numerical simulations for cell-cell communication

Paper II, it is implemented a comparative analysis between the experimental observations and the behavior predicted by the implementation of the biological model for single-cell yeast glycolysis [18]. For this purpose, an array of 210 circular geometries were introduced in the COMSOL simulations previously mentioned for the "5-in-1" diffusion chambers.

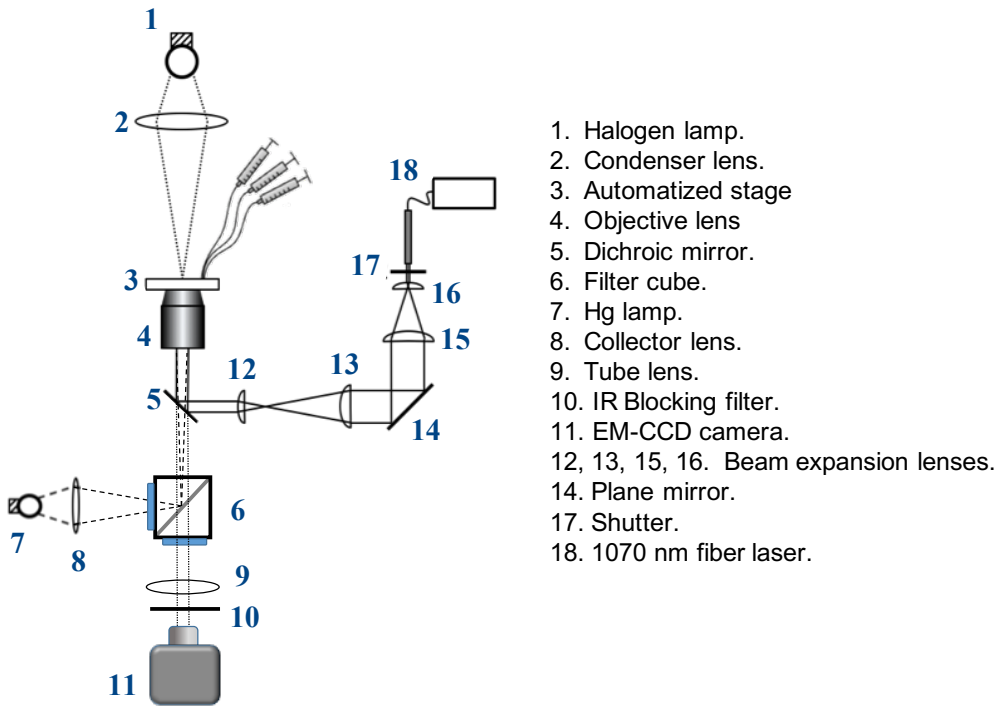

Figure 4.5: Schematic of the optical system. Transmission images in real time using the halogen lamp, are used as feedback for the cell positioning stage with the optical tweezers or when loading the diffusion chambers. Fluorescence images are obtained by exciting the sample and collecting the emission through the same objective lens.

Each of these circles emulate a single yeast cell, with the boundary conditions determined by the diffusion coefficients of the cell membranes (see Methods section in **Paper II**). Additionally, A set of ordinary differential equations (ODEs), present in the kinetic model for the single-cell yeast glycolytic cycle, were assigned to calculate all the reactions taking place inside all the cell domains. In this way, the intracellular network is coupled with the extracellular conditions to simulate the interaction of individual cells with each other and with the controlled environment. In order to bring the simulations closer to the experimental conditions, cell heterogeneity was included in terms of cell size and the initial phase of the oscillations. For this purpose, randomized cell diameters were assigned to emulate yeast cell sizes at different ages. Internal parameters such as initial concentrations of intermediate metabolites were adjusted to obtain 10 different initial phase values scattered across the cell array. For this study, no additional parameters were modified from the original model.

For the synchronization simulations addressed in **Paper III**, the study of the glycolytic phase adaptation in relation to the intracellular reaction chain, required further characterization of the model parameters. Introducing additional cell heterogeneity in terms of the enzymatic concentrations rates that translate into different frequency values, allowed the evaluation of the synchronization mechanism robustness. Two scattered subpopulations

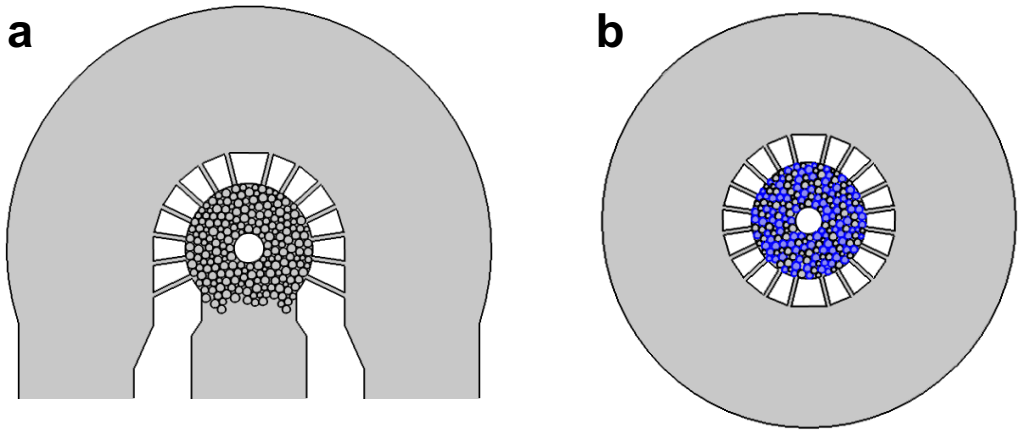

Figure 4.6: Architectures for cell-cell communication COMSOL simulations. In order to emulate the interactions between individual cells and with the environment, A total of 210 circular geometries where defined as the yeast cells, where each of them was assigned with an individual reaction chain corresponding to glycolysis. The cells were costrained in microfluidic environments where the diffusion and reaction rates aimed for describing the real conditions. (a) The device implemented in the experiments reported in **Paper II** was replicated to compare the synchronization communities and description of the synchronization waves. In (b) A new geometry is shown for the study reported in **Paper III**, where a theoretical characterization of the single-cell responses did not require inlets or outlets in the device. This design aimed to obtain radially symmetric diffusion gradients, therefore the outer boundary was defined as a concentration inlet and the inner circle as an open boundary for GLC, ACA, ETOH and CN^-. Here also the two scattered populations with different VmG3PDH values are displayed in blue and grey respectively.

were assigned with different values of the parameter VmG3PDH that corresponds to the concentration of the enzyme glycerol 3-phosphate dehydrogenase. The reaction rate given by this enzyme has shown to have the greatest influence in the frequency of the glycolytic oscillation [78], making it a suitable parameter to obtain subpopulations with different frequency values (see Figure 4.6). For all the simulations, probes for ACA, GLC, CN^- and ETOH were introduced to measure their concentrations for every time step, taking into account that these molecules interact both inside each cell and extracellularly.

Chapter 5

Data Analysis

Images acquired from the experiments were processed and analyzed to obtain time series coming from individual yeast cells. Periodic autofluorescence behavior was studied both in the time and frequency domains. The characterization of oscillatory parameters such as frequency and phase can give insight into the biological processes, chemical concentrations, and mechanisms involved in the metabolic responses. The raw data was processed focusing on the relevant spectral components to evaluate the oscillatory behavior due to glycolysis and avoid misleading trends. Moreover, in **Paper I** and **Paper II**, images were filtered to avoid noise and other artifacts. For each of the specific environmental and cell conditions, glycolytic synchronization was evaluated via cross-correlations and the standardized Kuramoto order parameter. Network analysis, together with graph theory, was implemented to characterize and visualize phase propagation and the spatial distribution of synchrony reported in **Paper II**. The data obtained from the numerical simulations was analyzed using the same methods as the experimental data to evaluate synchronization. In addition to the NADH signals obtained experimentally, the simulations provided time series for all the intermediate metabolites involved in the glycolytic pathway. The focus was centered on the spatio-temporal behaviour of the NADH, ACA and ETOH single-cell signals. The simulated single-cell metabolite signals obtained in **Paper III**, were treated to characterize synchronization waves based on the cells' position in the new geometric boundaries. The data analysis for the experimental data was also presented in the previous licentiate thesis [54].

5.1 Image processing

The processing of the acquired fluorescence image stacks was performed using a combination of the functions and toolboxes offered by the softwares ImageJ (https://imagej.nih.gov/ij/) and MATLAB®. When sensing weak fluorescence, it is necessary to adjust the camera settings such as the sensor gain and the exposure time in order to detect low-intensity signals. Images acquired with additional gain, amplify not only the expected signal but also the noise given by the background or the electronics. Long exposure times can give misleading information if the sample is not well fixed or the light source is not stable. The Kalman filter or Kalman prediction/correction algorithm is a powerfull tool to remove high gain noise from time-dependent stacks of images [79,80]. By setting the initial values

(from 0 to 1) of the filter gain, G, and noise variance estimate, V, one can adjust the sensitivity to momentary fluctuations and an estimated noise variance respectively. As a first step, V will be used as the error seed, E_k^-, that will be updated iteratively. In a similar way, the first image, I_k, will be used as the prediction seed I_k^-. For every image, the Kalman gain K_k is calculated as

$$K_k = \frac{E_k^-}{E_k^- + V} \tag{5.1}$$

and used to correct the next image and variance estimate. Hence, if K_k increases, it means that the measurements are accurate enough and the image update depends mostly on the measurements. On the other hand, when K_k decreases, the correction will depend mostly on the predictions as can be appreciated in

$$I_k = GI_k + (1 - G)M_k + K_k(M_k - I_k^-), \tag{5.2}$$

where M_k is the measure performed for each image and for the variance estimate

$$E_k = E_k^-(1 - K_k). \tag{5.3}$$

The prediction will be given by

$$I_{k+1}^- = I_k \; ; \; E_{k+1}^- = E_k \tag{5.4}$$

and the values will be updated by

$$I_k^- = I_{k+1}^- \; ; \; E_k^- = E_{k+1}^- \tag{5.5}$$

The Kalman filter was applied to all the raw images included in **Paper I** and **II**.

The images acquired from the "5-in-1" device were taken by moving the sample stage of the microscope to the positions of each chamber every 2 s (as mentioned in section 4.4). After every complete loop, the stage returned to the first location. However, the images showed slight misalignments that needed to be adjusted before setting a mask to follow each cell through the complete stack. For this purpose, a stabilizer function based on the Lucas-Kanade algorithm was implemented [81]. It aligns each of the images, $I(\mathbf{x})$, with a constantly updated template, $T(\mathbf{x})$, by finding the optimal warp, $W(\mathbf{x{:}p})$, where $\mathbf{x}$ is a vector containing the pixel coordinates and $\mathbf{p}$ is a vector with the warping parameters. For the 2D images, only translation of the pixels was implemented giving

$$W_{(x:p)} = \begin{bmatrix} x + p_1 \\ y + p_2 \end{bmatrix}. \tag{5.6}$$

The main goal of the algorithm is to minimize the sum of squared error between the

warped images and the template

$$\Sigma_x[I(W(\mathbf{x}:\mathbf{p}+\Delta\mathbf{p})-T(\mathbf{x}))]^2. \tag{5.7}$$

$\mathbf{p}$ starts from a seed value and updates iteratively as $\mathbf{p} \leftarrow \mathbf{p}+\Delta\mathbf{p}$ until the two images converge. The template also updates for every image using

$$T = a * T_0 + (1-a)I. \tag{5.8}$$

Where T_0 is the old template and a is the template update coefficient with values from 0 to 1. It is initially adjusted to determine how much the new template depends on on the old one.

5.2 Intercellular analysis

For the studies reported in **Paper I** and **Paper II**. Oval regions of interest (ROI) were defined around each cell as a mask for the complete stack of images. The mean intensity value corresponding to the individual cells for each frame was used to obtain the times series. An additional ROI was placed in a background region where no fluorescent activity took place to obtain a background signal. After extracting the time series, the background signal was subtracted from each cell's measured responses. The next step was to eliminate absolute intensity changes that differ from the periodicity range due to glycolytic oscillations. For this purpose, a running average was calculated using an average window of 55 samples and substracted from the original time series.

5.2.1 Order parameter

In order to evaluate the degree of synchrony based on a comparative analysis within the complete cell array presented in **Paper II**, it was necessary to evaluate the phase relations between different individual cells in the study. The Kuramoto model can provide a description of the coupling between oscillating cells using the order parameter defined as

$$r(t) = \left| \frac{1}{N} \Sigma_{n=1}^{N} e^{-i\Phi_n(t)} \right|, \tag{5.9}$$

Where N corresponds to the total number of cells in the chamber and Φ_n is the instant phase for each individual yeast cell in the array. Here, r is a normalized coefficient that quantifies the degree of synchrony from 0 to 1 depending on the number of coupled oscillating cells at each time point [43–45]. The instant phases of the glycolytic oscillation were obtained by calculating the Hilbert transform, which offers the possibility of dealing with real signals in the complex plane as

$$z(t) = z_R(t) + jz_i(t) = x(t) + j\mathscr{H}x(t). \tag{5.10}$$

Where x(t) is the real signal in the complex form z(t). In this way, the instant phase can be calculated as follows:

$$\Phi(t) = arctan\left[\frac{z_i(t)}{z_R(t)}\right]. \tag{5.11}$$

In **Paper II**, the order parameter is implemented to evaluate the time-dependent degree of synchronization between the individual cells in the array. Due to the global comparisonn based solely on the instantaneous phases, the spatial distribution of synchronization and possible phase relations required the additional signal treatment presented in the following subsection.

5.2.2 Synchronization communities

Due to each cell location and geometry constrains of the diffusion chambers in **Paper II**, the exposure to local environmental conditions revealed subpopulation couplings and spatial distribution of synchronization. Therefore, a method based on graph theory [46, 47] was implemented to identify and visualize these synchronized cell clusters. Individual oscillating cells were considered to be the nodes of a network where the connections were weighted based on Pearson cross-correlations at zero delay. Communities of cells were identified by implementing the Louvain modularity method [48]. The modularity describes how precise a network can be divided into communities. For this purpose, the density of connections within a community is calculated and then compares it with the density in a random network where the same number of connections are used. In this way, the Louvain method calculates the variations in modularity by initially assigning each cell to a different community and later moving a cell i to a neighbor community C. The variation in modularity M is calculated by

$$\Delta M = \left[\frac{\Sigma_{in} + 2k_{i,in}}{2W} - \left(\frac{\Sigma_{tot} + k_i}{2W}\right)^2\right] - \left[\frac{\Sigma_{in}}{2W} - \left(\frac{\Sigma_{tot}}{2W}\right)^2 - \left(\frac{k_i}{2W}\right)^2\right], \tag{5.12}$$

Σ_{in} is the sum of the weights inside C, Σ_{tot} is the sum of all the weights of connections coming to cells in C, k_i is the sum of the connection weights coming to cell i, $k_{i,in}$ is the sum of the weights for connections going from the cell i to the cells inside C and W is the sum of the weights in the complete network links. This process runs iteratively until no positive ΔM can be obtained further. Figure 5.1 shows a correlation matrix with all of the oscillating cells inside a diffusion chamber for the case of 12 mM CN^- exposure and the reorganization into synchronization communities in an adjacency matrix. With the assigned cell indices to each community, the spatial distribution of highly synchronized subpopulation was mapped for each of the CN^- exposures in **Paper II**.

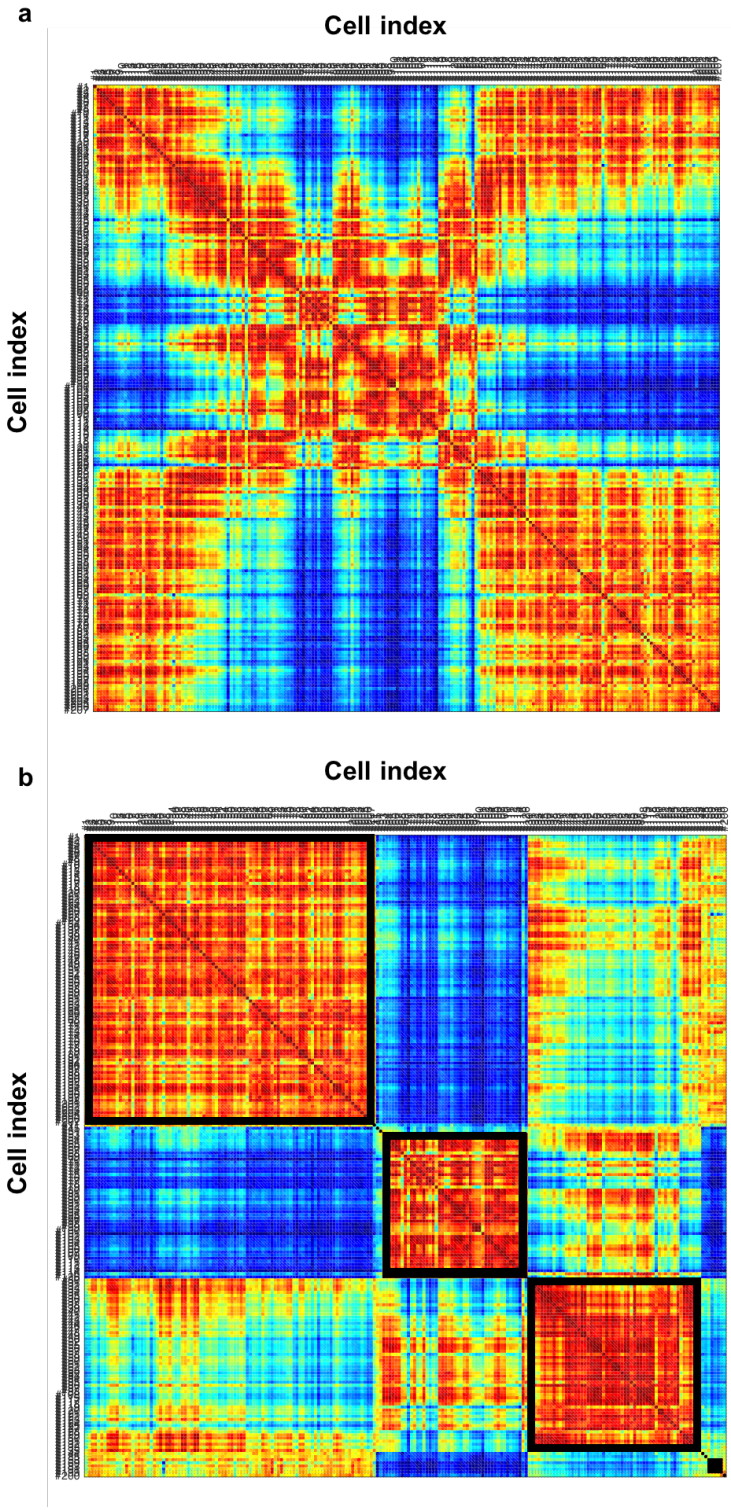

Figure 5.1: Symmetrical correlation matrices for experimental single-cell signals in a microfluidic chamber. a) 203 cells are organized by their index and weighted by a normalized cross-correlation. b) The cells are rearranged based on the communities' identification, using the Louvain modularity method with a Pearson correlation coefficient threshold of 0.7.

Delayed cross-correlations were calculated in order to find possible phase propagations or dependences inside the chamber. For this purpose, signals were correlated with shifts from -20 s to 20 s. In Figure 5.2 the Pearson coefficient is used to map the correlation levels between one yeast cell and the rest of the cells present in the chamber. In this way, high correlation levels in a specific delay suggest a phase relation and a possible wave propagation. In **Paper II** this same process was performed for a complete community previously calculated at zero delay to observe possible phase relations between communities. As it is shown in this paper, the spatial distribution of the communities elucidated the synchronization wavefront shape and the delayed correlations showed how they propagated. For this case, the mean value of the cross-correlations between the cells inside the community and the rest was mapped (See Figure 4 in **Paper II**).

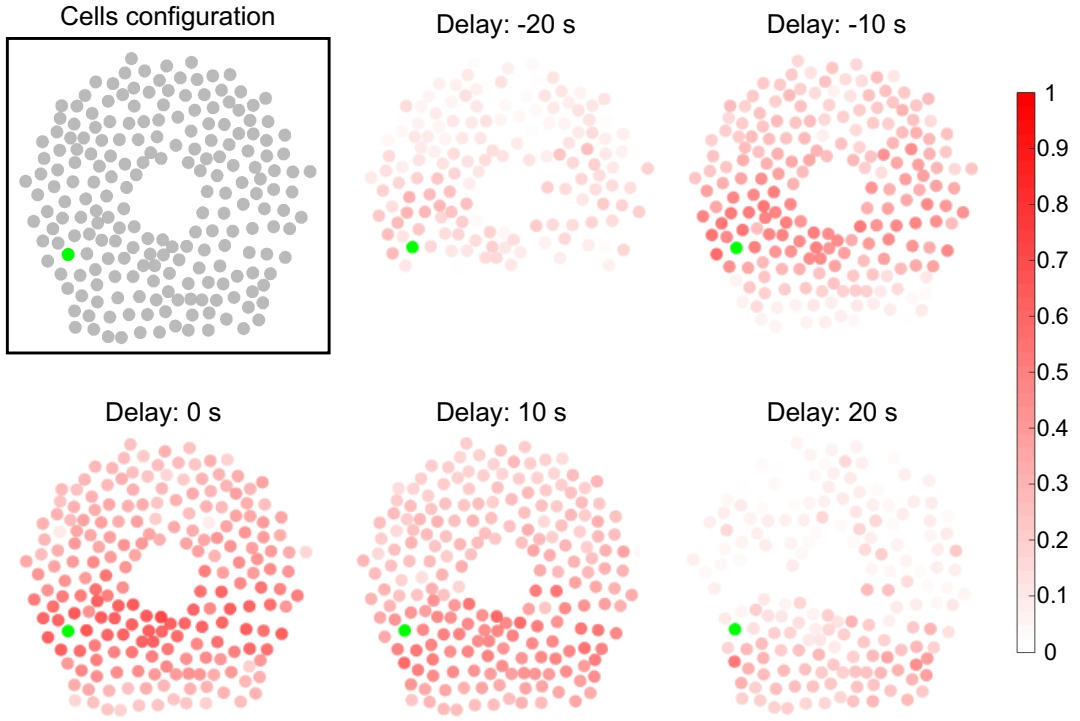

Figure 5.2: Delayed cross-correlations between cell #51 in the array and the rest of the cells present in the chamber. The mapping was performed based on the Pearson correlation coefficient. The evolution depending on the delay shows a phase propagation towards the bottom part of the chamber that suggests an influence from the diffusion of the GLC+CN^- stress and the secreted ACA.

5.2.3 Robustness analysis of the glycolytic synchronization waves

Paper III presents a deeper study on how synchronization waves can overcome the heterogeneity present in terms of the oscillatory frequency from each cell. For this purpose,

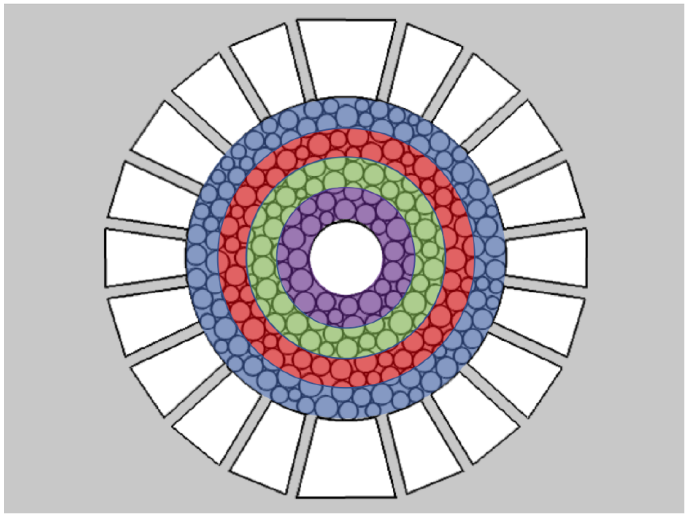

Figure 5.3: Simulated circular chamber with concentric subpopulation regions. To characterize the radial propagation of the synchronization waves, concentric ring-shaped regions were implemented to average the individual cell responses. The influence of the heterogeneity given by cells subpopulations oscillating with different natural frequencies on the synchronization wave, was studied by comparing its spatio-temporal evolution for each of the ring-shaped regions.

the results from the numerical simulations introducing a circular geometry and cell subpopulations with different natural frequencies were analyzed. Figure 5.3 shows the cells in the new geometry consisting of a radially symmetric chamber. The cell array was divided in concentric rings to average the local cell responses and observe the influence of individual signals on the wavefront. In **Paper III** ten ring contours were implemented. However, Figure 5.3 shows a case for only four concentric regions for a clearer display.

The time series for the ACA, NADH and ETOH simulated concentrations were analyzed in three separated intervals out of the 20 min observation to characterize time-dependent frequency changes. Figure 5.4 shows the control example for the simulated NADH signals, where cells with the same natural frequency are analyzed. Here, each color corresponds to a ring-shaped region where the relative delays confirm the radial propagation of the synchronization wave. The dominant frequency components are extracted for each interval using the Fourier transform to observe its time dependent evolution due to cell-cell coupling. In **Paper III**, this analysis was performed for the different configurations of frequency heterogeneity, and for the ACA waves as the chemical mediator between the individual cells.

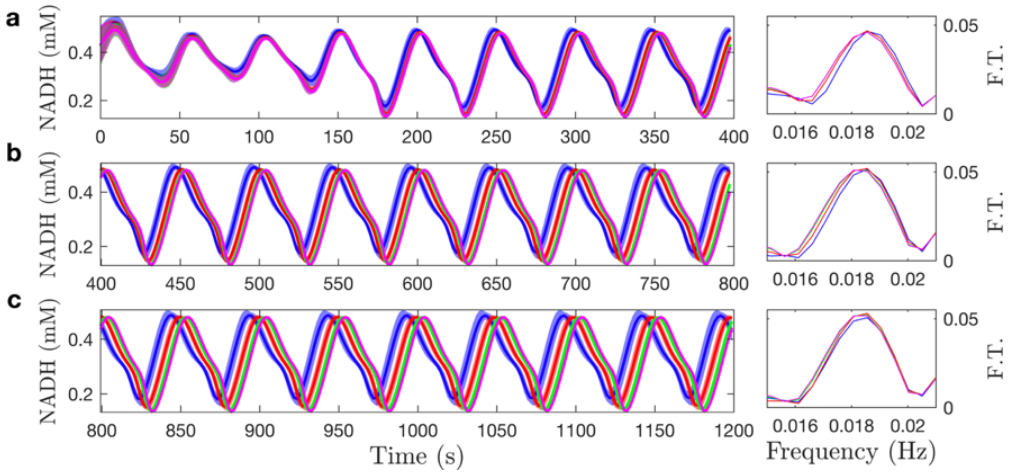

Figure 5.4: Time-dependent analysis of wave propagation through the concentric regions in the simulated symmetric cell chamber. The average NADH concentration fluctuations for each region are plotted were the shaded area correspond to the standard deviations. In the plots on the left side of the panel, the time evolution of the delays between the ring-shaped regions is shown for the three different intervals (a-c). The plots on the right side of the panel show the extracted dominant frequencies for each of the averaged regions. In this way, it is possible to observe any tendency of frequency stabilization among the cell regions. **Paper III** presents the case for ACA waves as the chemical mediator between the individual cells.

Chapter 6

Results and Discussion

6.1 Paper I: Design, fabrication and implementation of a diffusion chamber coupled with optical tweezers for glycolytic synchronization studies

A new microfluidic device was designed as a transition from previous experiments that focused on glycolytic oscillations at a single-cell level, to the scope of intercellular communication between individual cells. This system aimed to provide a diffusion-based transport of chemical species in order to guarantee cell-cell interactions by the exchange of ACA as the suggested chemical mediator. **Paper I** presents a microfluidic chamber that consists of a "U-shaped" flow-channel that surrounds a circular region, to which is connected by diffusion apertures. This configuration assured the reach of chemical inputs towards the center, minimizing convection in the area where cells are located. Optical tweezers were implemented similarly to previous experiments in flow-based chambers [9, 30], where individual yeast cells were captured and fixed in a controlled array prior to GLC and CN^- exposure. However, in this device, the cells were exposed to the stress solution under quasi-static conditions.

The hydrodynamic simulations' and fluoresceine experiments' results shown in **Paper I** proved diffusion transport of chemical species to be the dominant mechanism for stressing the cell array positioned inside the chamber. The microfluidic chamber was obtained with the required specifications using photolithography together with PDMS molding, and provided the conditions for the experimental procedure. The yeast cells were trapped, transported, and placed in a 4x4 rectangular array where the cells were exposed to GLC and CN^-. As can be seen in Figure 4 of **Paper I**, the single-cell NADH signals presented weak and non-sustained oscillations with spontaneous and synchronized amplitude bursts. As mentioned in previous studies [9,30], glycolytic oscillations in starved cells start with a glucose burst depending on concentration variations. However, in this experiment, these NADH peaks appeared isolated. These results suggest that cell-cell coupling can take place via ACA exchange by diffusion. Nonetheless, this microfluidic device required further optimization to guarantee sensitive control on the concentration gradients, and a

cellular arrangement that prevents secreted ACA to be diffused away. Additionally, future experimental investigation on the metabolic effects of having different ratios of GLC and CN^- in a quasi-static environment, can lead to the characterization of single-cell responses and cell-cell interactions as a function of the environmental conditions. This is addressed in the study presented in **Paper II**.

6.2 Paper II: Intercellular communication induces glycolytic synchronization waves between individually oscillating cells

Paper II proposed and implemented a methodology to characterize cell-cell interactions at a single-cell level. With a multichamber microfluidic chip, a compact monolayered array of cells was positioned to obtain a quasi-radial symmetry in environmental conditions minimizing free-media space. By using 2 μm apertures, diffusion coverage was optimized in comparison with the device reported in **Paper I**, and by reducing the chamber height to 5 μm the interaction between individual cells was restricted to lateral chemical exchange. Hydrodynamic simulations together with fluorescine experiments confirmed the chemical concentration distributions under quasi-static conditions. The "5-in-1" configuration allowed the simultaneous injection of cells from the same colony and the automatized measures of NADH fluorescence cell responses at different GLC and CN^- stress ratios. The time series were extracted from each cell present in the arrays and revealed sustained NADH oscillations when stressing the arrays of yeast cells by diffusion.

In contrast with population glycolytic synchronization studies, entrainment of individual neighboring yeast cells due to cell-cell interaction was measured for the first time in a microfluidic device. The calculation of the Kuramoto order parameter using the instantaneous phases confirmed the existence of different synchronized subpopulations distributed in the cell array. **Paper II** reports the implementation of graph theory to study and visualize the spatio-temporal distribution of synchronization across individual cells. To do this, the oscillating cells were considered as nodes of a network where the connections were weighted by the Pearson cross-correlation between their NADH signals. By implementing the Louvain method, variations in modularity served the purpose of identifying cell clusters or communities that could be grouped based on their synchronization, and mapped to visualize their spatial distribution.

The formation of synchronized communities was compared for the different GLC and CN^- ratios present in the "5-in-1" device. The results elucidated a spatio-temporal dependence of glycolytic synchronization as a function of the CN^- concentration gradients. Delayed cross-correlations showed relative delays between the NADH signals coming from cells in different locations, which provided a consistent evidence of intercellular glycolytic synchronization waves. Moreover, the propagation of these waves overcome the natural heterogeneity given by individual intracellular rates and extracellular local concentrations. The experimental results were compared with numerical simulations based on the experimental conditions of the experiments, and implemented a detailed kinetic model of glycolysis for individual yeast cells. Therefore, these results showed the link between the extracellular diffusion and reaction, with the intracellular glycolytic pathway of the

individual cells that resulted into synchronization waves.

The results from this study show good agreement with population experiments and core models on glycolytic synchronization waves, and bring one step further the understanding of the effect of heterogeneity on collective responses. Therefore, these findings can provide insight onto the role of glycolytic synchronization in other biological processes at single-cell level, such as the pulsatile insulin secretion from β cells the in pancreatic islets.

6.3 Paper III: Cell heterogeneneity affects the formation of glycolytic synchronization waves in yeast

This paper presents a set of numerical simulations to characterize the robustness of the glycolytic synchronization waves. In **Paper II**, there was experimental evidence that glycolytic synchronization waves overcome the high heterogeneity present in such a reduced population. However, the simulations presented to test the capacity of the biological model to explain synchronization lacked heterogeneity in terms of enzymatic rates in individual cells. Thus, the influence of frequency heterogeneity was not included. In order to characterize the glycolytic synchronization waves as a function of heterogeneity, the microfluidic chamber was modified aiming for a radially symmetric distribution of the concentration gradients. In this way, it was possible to average the cell responses over concentric loops in the cell chamber and describe the travelling waves for each radial distance. The frequency changes in the single-cell glycolytic oscillations were achieved by modifying the VmG3PDH parameter in the kinetic model. This parameter corresponds to the enzymatic rate of glyceraldehyde 3-phosphate dehydrogenase, which has shown to have the strongest influence on the glycolytic natural frequency [78].

In **Paper III** two scattered subpopulations of the cell array were assigned with different values of VmG3PDH, and the relative deviation of these values were implemented to characterize how the propagation of the synchronization waves was affected. The cell heterogeneity was quantified in terms of the standard deviation of the ACA concentrations for each of the averaged distances, and was plotted as a function of time. The results presented in this paper showed that depending on the ratio between the frequencies present in the subpopulations, sustained waves or periodic trains of pulses, propagate across the chamber. From the biological point of view, this suggests that there must be a threshold value for heterogeneity were cell can maintain synchronicity, where at ratios where the pulse trains are too far apart, the cell-cell coupling would lead to a steady state.

This study requires further investigation in order to bring a general description on how the spatio-temporal dynamics are affected by realistic heterogeneities. Moreover, it requires to expand the spatial characterization of the herogeneity to different type of cell distributions in the chamber, going from small scattered clusters with anomalous frequencies, to well-limited regions. In this way, one could characterize how glycolytic synchronization is disrupted in similar real configurations such as the pancreatic islets.

Chapter 7

Conclusions and Outlook

In this work, glycolytic oscillations, and subsequent synchronization were experimentally induced in yeast cells. By designing, fabricating and implementing custom microfluidic chambers, sensitive environmental control and cell handling was achieved, where cell-cell interactions were characterized from single-cell responses. The parameters involved in the experimental procedures, such as stress concentration ratios and diffusion gradients, were optimized to observe glycolytic synchronization waves and subpopulation entrainment.

Graph theory provided a novel tool to analyze the spatio-temporal distribution of the single-cell responses, allowing to extract information about the collective behavior. The identification of synchronization communities and the calculation of delayed correlations provided insight on how individually oscillating cells transition to coupled states. The numerical simulations presented in this thesis permitted the integration of the kinetic model for glycolysis previously developed for individual yeast cells, with the environmental conditions involved in cell-cell communication. As a result, the experimental observations were corroborated from a theoretical perspective.

The results presented in this thesis are in accordance with previous studies at a population level, where glycolytic synchronization waves were observed as a result of diffusion-based cell-cell communication. Furthermore, the single-cell approach implemented to study a collective behavior contributes to the understanding of heterogeneity in coordinated biological processes. For example, β-cells, which are required to synchronize a pulsatile insulin secretion in the pancreatic islets.

As future prospects of this work, experimental optimization of the microfluidic devices can bring the possibility to test synchronization in mammalian cells. Moreover, the methodology developed here could be extrapolated to study β-cells and move towards a first approach of a pancreas-on-chip. Similarly, the numerical simulations can integrate the coupled pathways involved in insulin secretion to obtain a detailed pancreatic synchronization model, able to describe islets under healthy conditions, and to simulate abnormal behaviour related to metabolic diseases such as Type II diabetes.

Acknowledgements

Now that I am finally completing this long journey, I would like to start by thanking my main supervisor Mattias Goksör for providing me with all the required means to develop my PhD and for helping me to structure my work.

I would like to give special thanks to my co-supervisor Caroline B. Adiels for all the academic and personal guidance through all this time, but mainly for being the kindest person I have ever encounter in a workplace.

I would also like to thank the other members of the Biological Physics group. To Philip Dalsbecker, Asim Faridi and Zofia Korczak for always having a good attitude towards me and helping me out every time I needed it. It was a very nice experience to share office with you guys. To all the members of the Soft Matter group: Giovanni Volpe who was crucial in the process to complete my research. To Falko, Laura, Aykut, Saga, Alessandro and Mite, for all the nice moments at work and outside as well. I wish you all the best.

I want to give special thanks to my family: my mother and my grandmother who always reminded me what is really important in life. Minin y Ceci, las quiero mucho.

Last but not least, to my life partner and biggest support, Lize de Coster. Thank you for giving me the strength and motivation I need everyday. Te amo.

Göteborg, November 1, 2019
Martin Mojica Benavides

References

[1] V. E. Deneke and S. Di Talia, Chemical waves in cell and developmental biology, *The Journal of Cell Biology* **217**, 1193–1204 (2018).

[2] P. Richard, The rhythm of yeast., *FEMS Microbiol Rev* **27**, 547–557 (2003).

[3] S. Gilroy, K. Trebacz, and V. Salvador-Recatala, Editorial: Inter-cellular Electrical Signals in Plant Adaptation and Communication., *Front Plant Sci* **9**, 643 (2018).

[4] C. M. Waters and B. L. Bassler, QUORUM SENSING: Cell-to-Cell Communication in Bacteria, *Annual Review of Cell and Developmental Biology* **21**, 319–346 (2005). PMID: 16212498.

[5] G. Banfalvi, *Overview of Cell Synchronization*, pages 1–23, Humana Press, Totowa, NJ (2011).

[6] A. Betz and J. U. Becker, Phase dependent phase shifts induced by pyruvate and acetaldehyde in oscillating NADH of yeast cells, *Journal of Interdisciplinary Cycle Research* **6**, 167–173 (1975).

[7] P. Richard, B. M. Bakker, B. Teusink, K. Van Dam, and H. V. Westerhoff, Acetaldehyde mediates the synchronization of sustained glycolytic oscillations in populations of yeast cells., *European Journal of Biochemistry* **235**, 238–241 (1996).

[8] R. Bertram, A. Sherman, and L. S. Satin, Metabolic and electrical oscillations: partners in controlling pulsatile insulin secretion., *Am J Physiol Endocrinol Metab* **293**, E890–900 (2007).

[9] A.-K. Gustavsson, C. B. Adiels, B. Mehlig, and M. Goksör, Entrainment of heterogeneous glycolytic oscillations in single cells, *Scientific Reports* **5**, 9404 EP – (2015).

[10] K. Tornheim, Are metabolic oscillations responsible for normal oscillatory insulin secretion?, *Diabetes* **46**, 1375–1380 (1997).

[11] F. Hynne, S. Dano, and P. G. Sorensen, Full-scale model of glycolysis in Saccharomyces cerevisiae., *Biophys Chem* **94**, 121–163 Dec 2001.

[12] G. H. Patterson, S. M. Knobel, P. Arkhammar, O. Thastrup, and D. W. Piston, Separation of the glucose-stimulated cytoplasmic and mitochondrial

NAD(P)H responses in pancreatic islet cells, *Proceedings of the National Academy of Sciences* **97**, 5203–5207 (2000).

[13] A. Ghosh and B. Chance, Oscillations of glycolytic intermediates in yeast cells, *Biochemical and Biophysical Research Communications* **16**, 174 – 181 (1964).

[14] S. H. Krebs, J. J. Kay, and P. D. J. Weitzman. Krebs' citric acid cycle : half a century and still turning (1987). Symposium was held at University of Leicester, Apr. 1987.

[15] C. to volume, Methods in Enzymology, In *Citric Acid Cycle*, volume 13 of *Methods in Enzymology*, pages v – viii, Academic Press (1969).

[16] M. Bier, B. M. Bakker, and H. V. Westerhoff, How yeast cells synchronize their glycolytic oscillations: a perturbation analytic treatment., *Biophysical Journal* **78**, 1087–1093 (2000).

[17] S. Danø, F. Hynne, S. De Monte, F. d'Ovidio, P. G. Sorensen, and H. Westerhoff, Synchronization of glycolytic oscillations in a yeast cell population, *Faraday Discuss.* **120**, 261–275 (2002).

[18] F. B. du Preez, D. D. van Niekerk, B. Kooi, J. M. Rohwer, and J. L. Snoep, From steady-state to synchronized yeast glycolytic oscillations I: model construction, *The FEBS Journal* **279**, 2810–2822 (2012).

[19] A. Betz and B. Chance, Influence of inhibitors and temperature on the oscillation of reduced pyridine nucleotides in yeast cells, *Archives of Biochemistry and Biophysics* **109**, 579 – 584 (1965).

[20] B. O. Hald, M. Smrcinova, and P. G. Sorensen, Influence of cyanide on diauxic oscillations in yeast., *FEBS J* **279**, 4410–4420 Dec 2012.

[21] L. Duysens and J. Amesz, Fluorescence spectrophotometry of reduced phosphopyridine nucleotide in intact cells in the near-ultraviolet and visible region, *Biochimica et Biophysica Acta* **24**, 19 – 26 (1957).

[22] F. Hommes, Oscillatory reductions of pyridine nucleotides during anaerobic glycolysis in brewers' yeast, *Archives of Biochemistry and Biophysics* **108**, 36 – 46 (1964).

[23] A. Betz and B. Chance, Phase relationship of glycolytic intermediates in yeast cells with oscillatory metabolic control, *Archives of Biochemistry and Biophysics* **109**, 585 – 594 (1965).

[24] B. Hess and A. Boiteux, Mechanism of glycolytic oscillation in yeast. I. Aerobic and anaerobic growth conditions for obtaining glycolytic oscillation., *Hoppe Seylers Z Physiol Chem* **349**, 1567–1574 (1968).

[25] A. Goldbeter and S. R. Caplan, Oscillatory Enzymes, *Annual Review of Biophysics and Bioengineering* **5**, 449–476 (1976). PMID: 182066.

[26] A. Boiteux and B. Hess, Design of glycolysis, *Philosophical Transactions of the Royal Society of London B: Biological Sciences* **293**, 5–22 (1981).

[27] B. Hess, The glycolytic oscillator., *J Exp Biol* **81**, 7–14 (1979).

[28] K. Pye and B. Chance, Sustained sinusoidal oscillations of reduced pyridine nucleotide in a cell-free extract of Saccharomyces carlsbergensis, *Proceedings of the National Academy of Sciences* **55**, 888–894 (1966).

[29] A. Weber, Y. Prokazov, W. Zuschratter, and M. J. B. Hauser, Desynchronisation of Glycolytic Oscillations in Yeast Cell Populations, *PLOS ONE* **7**, 1–8 (2012).

[30] A.-K. Gustavsson, D. D. van Niekerk, C. B. Adiels, F. B. du Preez, M. Goksör, and J. L. Snoep, Sustained glycolytic oscillations in individual isolated yeast cells, *FEBS Journal* **279**, 2837–2847 (2012).

[31] A. Weber, Y. Prokazov, W. Zuschratter, and M. J. B. Hauser, *From Synchronised to Desynchronised Glycolytic Oscillations in Individual Yeast Cells*, pages 239–254, Springer International Publishing, Cham (2018).

[32] T. Amemiya, K. Obase, N. Hiramatsu, K. Itoh, K. Shibata, M. Takinoue, T. Yamamoto, and T. Yamaguchi, Collective and individual glycolytic oscillations in yeast cells encapsulated in alginate microparticles, *Chaos: An Interdisciplinary Journal of Nonlinear Science* **25**, 064606 (2015).

[33] A. K. Poulsen, M. Ø. Petersen, and L. F. Olsen, Single cell studies and simulation of cell–cell interactions using oscillating glycolysis in yeast cells, *Biophysical Chemistry* **125**, 275 – 280 (2007).

[34] A.-K. Gustavsson, D. D. van Niekerk, C. B. Adiels, B. Kooi, M. Goksor, and J. L. Snoep, Allosteric regulation of phosphofructokinase controls the emergence of glycolytic oscillations in isolated yeast cells., *FEBS Journal* **281**, 2784–2793 (2014).

[35] S. Danø, M. F. Madsen, and P. G. Sørensen, Quantitative characterization of cell synchronization in yeast, *Proceedings of the National Academy of Sciences of the United States of America* **104**, 12732–12736 (2007).

[36] D. van Niekerk, A.-K. Gustavsson, M. Mojica-Benavides, C. B. Adiels, M. Goksor, and J. L. Snoep, Phosphofructokinase controls the acetaldehyde induced phase shift in isolated yeast glycolytic oscillators, *Biochemical Journal* (2019).

[37] A. Boiteux and B. Hess, Spatial Dissipative Structures in Yeast Extracts, *Berichte der Bunsengesellschaft für physikalische Chemie* **84**, 392–398 (1980).

[38] S. Bagyan, T. Mair, E. Dulos, J. Boissonade, P. D. Kepper, and S. C. Müller, Glycolytic oscillations and waves in an open spatial reactor: Impact of feedback regulation of phosphofructokinase, *Biophysical Chemistry* **116**, 67 – 76 (2005).

[39] H. Jacobsen, H. Busse, and B. Havsteen, Spontaneous spatio-temporal organization in yeast cell suspension, *Journal of Cell Science* **43**, 367–377 (1980).

[40] J. Bolyó, T. Mair, G. Kuncová, and M. J. Hauser, Spatiotemporal dynamics of glycolytic waves provides new insights into the interactions between immobilized yeast cells and gels, *Biophysical Chemistry* **153**, 54 – 60 (2010).

[41] J. Schütze, T. Mair, M. J. Hauser, M. Falcke, and J. Wolf, Metabolic Synchronization by Traveling Waves in Yeast Cell Layers, *Biophysical Journal* **100**, 809 – 813 (2011).

[42] J. Schutze and J. Wolf, Spatio-temporal dynamics of glycolysis in cell layers. A mathematical model., *Biosystems* **99**, 104–108 Feb 2010.

[43] Y. Kuramoto, Self-entrainment of a population of coupled non-linear oscillators, In H. Araki, editor, *International Symposium on Mathematical Problems in Theoretical Physics*, pages 420–422, Berlin, Heidelberg (1975). Springer Berlin Heidelberg.

[44] S. Shinomoto and Y. Kuramoto, Phase Transitions in Active Rotator Systems, *Progress of Theoretical Physics* **75**, 1105–1110 (1986).

[45] S. H. Strogatz, From Kuramoto to Crawford: exploring the onset of synchronization in populations of coupled oscillators, *Physica D Nonlinear Phenomena* **143**, 1–20 (2000).

[46] V. D. Blondel, J.-L. Guillaume, R. Lambiotte, and E. Lefebvre, Fast unfolding of communities in large networks, *Journal of Statistical Mechanics: Theory and Experiment* **2008**, P10008 (2008).

[47] S. Fortunato, Community detection in graphs, *Physics Reports* **486**, 75 – 174 (2010).

[48] M. Mijalkov, E. Kakaei, J. B. Pereira, E. Westman, and G. Volpe, BRAPH: A graph theory software for the analysis of brain connectivity, *PLOS ONE* **12**, 1–23 (2017).

[49] R. Frenkel, Control of reduced diphosphopyridine nucleotide oscillations in beef heart extracts: II. Oscillations of glycolytic intermediates and adenine nucleotides, *Archives of Biochemistry and Biophysics* **125**, 157 – 165 (1968).

[50] K. Ibsen and K. Schiller, Oscillations of nucleotides and glycolytic intermediates in aerobic suspensions of Ehrlich ascites tumor cells, *Biochimica et Biophysica Acta (BBA) - Bioenergetics* **131**, 405 – 407 (1967).

[51] M. J. Merrins, A. R. Van Dyke, A. K. Mapp, M. A. Rizzo, and L. S. Satin, Direct Measurements of Oscillatory Glycolysis in Pancreatic Islet -Cells Using Novel Fluorescence Resonance Energy Transfer (FRET) Biosensors for Pyruvate Kinase M2 Activity, *Journal of Biological Chemistry* **288**, 33312–33322 (2013).

[52] D. R. Matthews, B. A. Naylor, R. G. Jones, G. M. Ward, and R. C. Turner, Pulsatile Insulin Has Greater Hypoglycemic Effect Than Continuous Delivery, *Diabetes* **32**, 617–621 (1983).

[53] T. Suzuki, T. Kanamori, and S. Inouye, Quantitative visualization of synchronized insulin secretion from 3D-cultured cells, *Biochemical and Biophysical Research Communications* **486**, 886 – 892 (2017).

[54] M. Mojica-Benavides, *Glycolytic synchronization in yeast: Single-cell studies in a microfluidic environment*, Licentiate thesis, University of Gothenburg, Gothenburg, Sweden (2018).

[55] A. Ashkin, Acceleration and Trapping of Particles by Radiation Pressure, *Phys. Rev. Lett.* **24**, 156–159 (1970).

[56] O. M. M. Philip H. Jones and G. Volpe, *Optical tweezers principles and applications*, Cambridge University Press (2015).

[57] E. Hecht, *Optics*, Addison-Wesley (2002).

[58] A. Ashkin, J. M. Dziedzic, and T. Yamane, Optical trapping and manipulation of single cells using infrared laser beams, *Nature* **330**, 769 EP – (1987).

[59] H. Zhang and K.-K. Liu, Optical tweezers for single cells, *Journal of the Royal Society Interface* **5**, 671–690 (2008).

[60] D. G. Grier, A revolution in optical manipulation, *Nature* **424**, 810 EP – (2003).

[61] E. Eriksson, K. Sott, F. Lundqvist, M. Sveningsson, J. Scrimgeour, D. Hanstorp, M. Goksor, and A. Graneli, A microfluidic device for reversible environmental changes around single cells using optical tweezers for cell selection and positioning., *Lab Chip* **10**, 617–625 (2010).

[62] P. Tabeling, *Introduction to Microfluidics*, Oxford University Press, New York, USA (2005).

[63] C. Crowe, D. Elger, and J. Roberson, *Engineering fluid mechanics*, Wiley (2000).

[64] G. Batchelor, *An Introduction to Fluid Dynamics*, Cambridge Mathematical Library, Cambridge University Press (2000).

[65] D. Tritton, *Physical Fluid Dynamics*, The Modern University in Physics Series, Springer Netherlands (2012).

[66] D. J. Beebe, G. A. Mensing, and G. M. Walker, Physics and applications of microfluidics in biology., *Annu Rev Biomed Eng* **4**, 261–286 (2002).

[67] C. Nordling and J. Österman, *Physics handbook for science and engineering*, Chartwell-Bratt (1999).

[68] S. Patankar, *Numerical Heat Transfer and Fluid Flow*, Electro Skills Series, Hemisphere Publishing Corporation (1980).

[69] N. Nguyen and S. Wereley, *Fundamentals and Applications of Microfluidics*, Artech House MEMS library, Artech House (2002).

[70] R. Martinez-Duarte and M. Madou. SU-8 Photolithography and Its Impact on Microfluidics 09 2010.

[71] T. Fujii, PDMS-based microfluidic devices for biomedical applications, *Microelectronic Engineering* **61-62**, 907 – 914 (2002). Micro- and Nano-Engineering 2001.

[72] S. K., E. E., and M. Goksor, Acquisition of single cell data in an optical microscope, *Lab on a Chip Technology: Biomolecular Separation and Analysis* pages 151–166 (2009).

[73] F. A. Chandra, G. Buzi, and J. C. Doyle, Glycolytic Oscillations and Limits on Robust Efficiency, *Science* **333**, 187–192 (2011).

[74] P. Richard, J. A. Diderich, B. M. Bakker, B. Teusink, K. van Dam, and H. V. Westerhoff, Yeast cells with a specific cellular make-up and an environment that removes acetaldehyde are prone to sustained glycolytic oscillations, *FEBS Letters* **341**, 223 – 226 (1994).

[75] null Ghauharali and null Brakenhoff, Fluorescence photobleaching-based image standardization for fluorescence microscopy, *Journal of Microscopy* **198**, 88–100.

[76] null Ghauharali, null Hofstraat, and null Brakenhoff, Fluorescence photobleaching-based shading correction for fluorescence microscopy, *Journal of Microscopy* **192**, 99–113.

[77] C. E. Shannon, Communication in the Presence of Noise, *Proceedings of the IRE* **37**, 10–21 (1949).

[78] T. Williamson, D. Adiamah, J.-M. Schwartz, and L. Stateva, Exploring the genetic control of glycolytic oscillations in Saccharomyces cerevisiae., *BMC Syst Biol* **6**, 108 Aug 2012.

[79] R. E. Kalman, A New Approach to Linear Filtering and Prediction Problems, *Journal of Basic Engineering* **82**, 35–45 03 1960.

[80] *Polynomial Kalman Filters*, pages 129–182, American Institute of Aeronautics and Astronautics (2009).

[81] K. Li. The image stabilizer plugin for ImageJ. http://www.cs.cmu.edu/ kangli/code/Image$_S tabilizer.html Feb.$2008.

[82] G. D. Gutierrez, J. Gromada, and L. Sussel, Heterogeneity of the Pancreatic Beta Cell, *Frontiers in Genetics* **8**, 22 (2017).